




Interdomain connecting loop and J loop structures determine cross-species compatibility of PCNA

Received for publication, May 3, 2021, and in revised form, June 17, 2021. Published, Papers in Press, June 25, 2021.
<https://doi.org/10.1016/j.jbc.2021.100911>

Premalata Kumari^{1,2,‡}, Rajivgandhi Sundaram^{3,4,‡}, Kodavati Manohar^{1,‡}, Dileep Vasudevan^{3,*} , and Narottam Acharya^{1,*} 

From the ¹Laboratory of Genomic Instability and Diseases, Department of Infectious Disease Biology, Institute of Life Sciences, Bhubaneswar, India; ²Regional Centre for Biotechnology, Faridabad, India; ³Laboratory of Macromolecular Crystallography, Department of Infectious Disease Biology, Institute of Life Sciences, Bhubaneswar, India; ⁴Manipal Academy of Higher Education, Manipal, India

Edited by Patrick Sung

Eukaryotic proliferating cell nuclear antigen (PCNA) plays an essential role in orchestrating the assembly of the replisome complex, stimulating processive DNA synthesis, and recruiting other regulatory proteins during the DNA damage response. PCNA and its binding partner network are relatively conserved in eukaryotes, and it exhibits extraordinary structural similarity across species. However, despite this structural similarity, the PCNA of a given species is rarely functional in heterologous systems. In this report, we determined the X-ray crystal structure of *Neurospora crassa* PCNA (NcPCNA) and compared its structure–function relationship with other available PCNA studies to understand this cross-species incompatibility. We found two regions, the interdomain connecting loop (IDCL) and J loop structures, vary significantly among PCNAs. In particular, the J loop deviates in NcPCNA from that in *Saccharomyces cerevisiae* PCNA (ScPCNA) by 7 Å. Differences in the IDCL structures result in varied binding affinities of PCNAs for the subunit Pol32 of DNA polymerase delta and for T2-amino alcohol, a small-molecule inhibitor of human PCNA. To validate that these structural differences are accountable for functional incompatibility in *S. cerevisiae*, we generated NcPCNA mutants mimicking IDCL and J loop structures of ScPCNA. Our genetic analyses suggested that NcPCNA mutants are fully functional in *S. cerevisiae*. The susceptibility of the strains harboring ScPCNA mimics of NcPCNA to various genotoxic agents was similar to that in yeast cells expressing ScPCNA. Taken together, we conclude that in addition to the overall architecture of PCNA, structures of the IDCL and J loop of PCNA are critical determinants of interspecies functional compatibility.

Proliferating cell nuclear antigen (PCNA) plays an essential role during DNA replication, repair, and recombination processes. Mostly, it acts as a docking platform for several proteins

involved in DNA synthesis, DNA damage response, chromatin assembly, cell cycle control, and chromatin remodeling and regulates their activities (1, 2). For example, PCNA physically interacts with the replicative DNA polymerase δ and enhances its nucleotide incorporation efficiency and processivity (3–5). PCNA is evolutionarily conserved not only in function but also in the structure across eukaryotic species. Despite the variation in amino acid sequences of PCNA from several different organisms, their overall atomic structures are markedly superimposed. PCNA has been characterized in humans, rats, budding and fission yeasts, protozoa, flies, *Arabidopsis*, and many archaeal species (2, 6). The crystal structures of PCNA from some of these organisms have also been determined (7–10). A typical eukaryotic PCNA consists of three protomers to form a toroidal-shaped structure with pseudo-6-fold symmetry that encircles the DNA double helix. Each PCNA protomer consists of two globular topologically identical domains connected by an interdomain connecting loop (IDCL). Considering remarkable PCNA structural and functional similarities, cross-species complementation of PCNA should be seemingly possible. However, it is hardly observed, as the function of a PCNA in a heterologous system mostly depends upon its affinity toward the PCNA-interacting peptide (PIP) box motif of cellular proteins involved in replication and repair. The PIP box present in the PCNA-binding partner moors into the hydrophobic cavity formed by the IDCL region. An earlier study classified fungal PCNAs into two compatible groups (11). Group I includes PCNA from *Saccharomyces cerevisiae*, *Candida* sp., *Kluyveromyces waltti*, *Ashbya gossypii*, and *Debaryomyces hansenii* and group II from *Schizosaccharomyces pombe*, *Yarrowia lipolytica*, *Neurospora crassa*, and *Aspergillus fumigatus*. IDCL and the C-terminal tail of PCNA, which are involved in PCNA–protein interaction, are highly conserved in their respective groups (Fig. S1A). Based on the sequence alignment, human PCNA could also be placed in group II. It was suggested that the interspecies compatibility of PCNAs only exists within the specific group. PCNAs belonging to group II will not functionally replace PCNA in group I species and *vice versa* (11).

To understand species specificity of PCNA and its functional compatibility across fungal species in greater detail, we

[‡] These authors contributed equally to this work.

* For correspondence: Narottam Acharya, narottam74@gmail.com, narottam_acharya@ils.res.in; Dileep Vasudevan, dileepvasudevan@gmail.com, dileep@ils.res.in.

Present address for Kodavati Manohar: Department of Neurosurgery, Center for Neuroregeneration, Houston Methodist Research Institute, Houston, Texas 77030, USA.

Three-dimensional structure of NcPCNA

have characterized PCNA from *N. crassa* and compared it with PCNA from *S. cerevisiae*, and the pathogenic yeasts *Candida albicans* and *A. fumigatus* (6, 9, 10), two representatives from each compatible groups. Although *C. albicans* PCNA (CaPCNA) possesses significant IDCL sequence identity and belongs to group I, contrary to the earlier report, CaPCNA is functionally noncompatible in *S. cerevisiae* (6, 9, 11). Our comparative structural analyses revealed that CaPCNA displayed noticeable structural alterations in the hydrophobic pocket, J loop, and P loop regions (9). While the IDCL and J-loop of PCNA are involved in ligand interaction, the P loop plays a regulatory role by undergoing post-translational modifications. Therefore, to understand the precise roles of IDCL and J loop in determining species specificity, herein, we expressed, purified, and determined the crystal structure of *N. crassa* PCNA (NcPCNA) and characterized its function in *S. cerevisiae*. Our biochemical and X-ray structure analyses suggested that NcPCNA also forms a homotrimeric ring. The overall three-dimensional architectures of these fungal PCNAs are very similar. However, similar to CaPCNA, NcPCNA also exhibits structural variations in the IDCL and J loop regions.

Our genetic analyses suggested that although NcPCNA can rescue the loss of function of *S. cerevisiae* PCNA (ScPCNA) in *S. cerevisiae*, it is inefficient in carrying out DNA replication and repair. Our mutational analyses further confirmed that IDCL and J loop structures are critical in determining the functional specificity of PCNA. Taken together, we suggest that PCNA is a highly species-specific protein. Despite similar architecture among PCNAs, certain unique structural elements such as IDCL and J loop determine interspecies compatibility.

Results

Identification of NcPCNA and sequence analyses

To identify a putative homologue of ScPCNA in *N. crassa*, we searched its genome database (<http://www.broad.mit.edu/annotation/genome/neurospora/Home.html>) by BLAST. The search identified the NcPCNA homologue that corresponds to *pcn* (Gene I.D.: NCU09239 and Protein I.D.:XP_964674.1) in the database with a score of $4e^{-86}$, identity of 47%, and similarity of 69% (Fig. 1). The putative NcPCNA amino acid

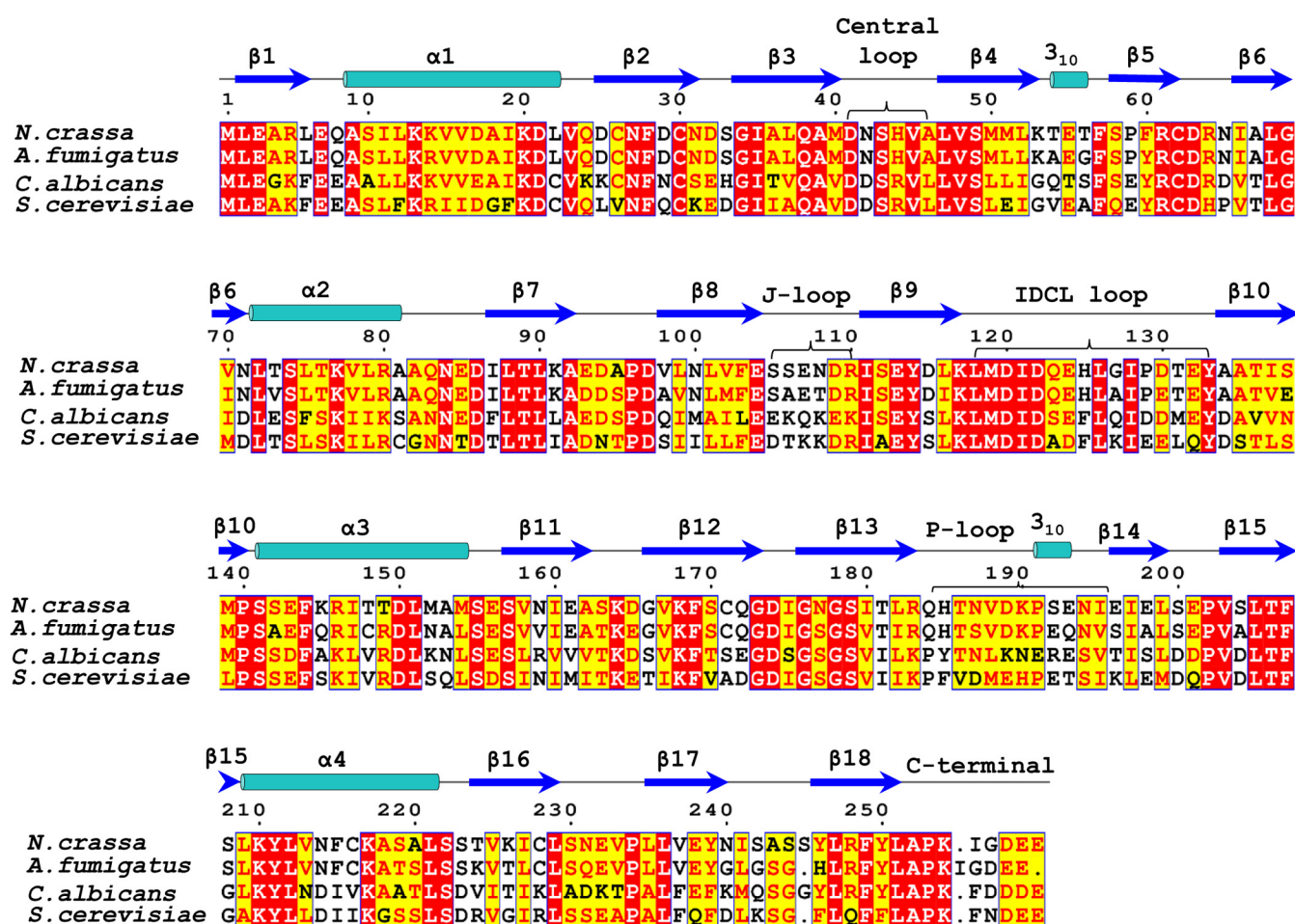


Figure 1. Multiple sequence alignment of two representative fungal PCNAs from group I and group II. Multiple sequence alignment of PCNA from *Candida albicans* (Q5AMN0), *Aspergillus fumigatus* (A0A0J5JF1), *Saccharomyces cerevisiae* (P15873), and *Neurospora crassa* (Q75F71) was performed using the T-Coffee web server, and the resulting alignment was rendered through ESPrpt. The secondary structural features for *N. crassa* PCNA are indicated above the alignment, wherein a helices are given as cylinders and beta-strands are marked as arrows. The central loop, IDCL, J loop, P loop, and the C-terminal tail are highlighted with a right brace and are labeled. IDCL, interdomain connecting loop; PCNA, proliferating cell nuclear antigen.

sequence showed homology with a score of $2e^{-157}$, identity of 80%, and similarity of 91%, and homology with a score of $2e^{-92}$, identity of 49%, and similarity of 72% with *A. fumigatus* PCNA (AfPCNA) and CaPCNA sequences, respectively. Interestingly, unlike in other known fungal species, the *pcn* gene carries two extreme end introns juxtaposed between the exons (Fig. S1C). In the 949 nucleotides of gene sequence, intron 1 and intron 2 are located from 45 to 140 nts and 859 to 931 nts, respectively. The three-dimensional structures are known for the other three fungal PCNAs, but not for NcPCNA. The amino acid sequence alignment suggests that NcPCNA possesses all the critical structural regions such as the central loop, J loop, IDCL, P loop, and the C-terminal tail required for the conserved functions of PCNA. Among these loops, the J loop located in the dimeric interface highly diverges among the PCNA from different species. Similarly, in the IDCL, of 16 residues, four residues (Q123, H125, G/A127, and P129) are different in NcPCNA and AfPCNA, compared with those in ScPCNA (Fig. S1A). The remaining 12 residues of the IDCL are either identical or conserved. Because the IDCL is involved in critical interactions with DNA polymerases and other DNA transaction proteins and the J loop in PCNA trimerization, whether the residue variations in these two loops of NcPCNA will lead to functional differences among the PCNAs made us investigate this protein further. Nevertheless, it is apparent from the sequence alignments that NcPCNA and AfPCNA diverge from ScPCNA and CaPCNA. Therefore, they have been rightly placed in different compatible groups (11).

NcPCNA forms a stable homotrimer

The J loop is formed by the residues between the β -strands β_8 and β_9 and plays an important role in intersubunit interactions and stabilization of the homotrimeric architecture of PCNA. Earlier studies on two mutants of ScPCNA (G178S and E113G) with altered J loop conformations revealed that deformation of the J loop weakens the intermolecular interaction and results in monomeric or dimeric PCNA *in vitro* (12, 13). Because we noticed amino acid variations in the J loop region of NcPCNA, to characterize NcPCNA further, the protein was purified using an amino-terminal glutathione-S-transferase (GST)-tag expression vector from bacterial cells. Similarly, the WT and G178S mutant of ScPCNA were also purified to near homogeneity (Fig. 2A). NcPCNA encodes a predicted 28.64-kDa protein composed of 259 amino acids and is one residue longer than ScPCNA (28.9 kDa) at its carboxyl terminus. Surprisingly, despite having almost similar molecular mass, NcPCNA showed abnormal mobility and migrated slower than the WT and G178S mutant of ScPCNAs in SDS-PAGE (Fig. 2A, compare lane 4 with lanes 2 and 3). However, in a non-denaturing condition where proteins migrate based on their mass and isoelectric point, both NcPCNA (\sim 29 kDa, pI 4.42) and WT ScPCNA (\sim 29 kDa, pI 4.51) migrated at a similar position (Fig. 2B, compare lane 2 with lanes 1 and 3). As reported earlier, the ScPCNA G178S mutant migrates faster than the WT ScPCNA in its monomeric form (Fig. 2B, lane 2). These results suggested that, like ScPCNA, NcPCNA also exists as a homotrimer in the solution. At 2 M urea,

ScPCNA trimer destabilizes and breaks down to monomeric forms of PCNA. Interestingly, NcPCNA did not form smaller subunits; instead, it showed aggregation or higher-order oligomerization (Fig. 2C, compare lane 3 with lanes 1 and 2). This observation was further supported by analytical size-exclusion chromatography, where NcPCNA eluted differently with and without 2 M urea (Fig. 2D). In the presence of urea, NcPCNA eluted early at \sim 1.4 ml elution volume (red line), suggesting higher molecular weight forms of PCNA; however, in the absence of urea, it eluted at \sim 1.6-ml elution volume, where trimeric ScPCNA also elutes. Taken together, this result suggested that despite amino acid variation in the J loop, in the native state, NcPCNA exists as a homotrimer. However, in the presence of denaturants such as SDS or 2 M urea, NcPCNA exhibits abnormal property and migrates differently.

Structure determination and structural features of NcPCNA

To understand the structure–function relationship, NcPCNA was purified and crystallized and the crystal structure solved. The NcPCNA crystal belonged to the space group *H3*, wherein the asymmetric unit (ASU) contained a single monomer of NcPCNA. The structure was solved using molecular replacement with AfPCNA structure as the search model (PDB ID: 5TUP) (10). The structure was solved to 1.95 Å resolution, and the structure refinement statistics are given in Table 1. Upon operating crystallographic symmetry, the structure revealed a trimeric organization characteristic of PCNA.

Structural analysis revealed that NcPCNA has a conserved canonical PCNA fold and displayed a pseudo-6-fold symmetry (Fig. 3, A and B). NcPCNA forms a trimer in crystal structure and also in the solution, which is consistent with other eukaryotic PCNAs (Fig. 3C). The structural superimposition of NcPCNA with AfPCNA, CaPCNA, and ScPCNA revealed that NcPCNA shares a high degree of structural similarity with RMSD values of 0.65 Å, 0.62 Å, and 1.3 Å, respectively. PDBE-PISA web server was used to analyze the interface and the assembly state of NcPCNA. The buried surface area at the interface of NcPCNA is 725 Å², and that is comparable with the values for CaPCNA (720 Å²), AfPCNA (656 Å²), and ScPCNA (654 Å²). Each NcPCNA protomer consists of two domains, A and B (Fig. 3D). The N-terminal region (residues Met1 to Lys117) forms domain A and is interlinked to domain B (residues Ala134 to Glu259) at the C terminus by a dynamic IDCL made up of residues Leu117 to Tyr133. Domains A (β 1- α 1- β 2- β 3- β 4- β 5- β 6- α 2- β 7- β 8- β 9) and B (β 10- α 3- β 11- β 12- β 13- β 14- β 15- α 4- β 16- β 17- β 18) shared nearly an identical topology. The central channel of the NcPCNA revealed a positively charged lining because of the presence of basic residues, mostly lysine and a few arginine residues, probably involved in the interaction with DNA as has been shown in other PCNAs (Fig. S2, A and B). These residues (K13, K14, K20, K77, R80, R146, K210, and K217) are also conserved in PCNAs from other organisms. The function of PCNA is also modulated through post-translational modifications (14). In many PCNA sequences, Lys117, Lys164, and Lys168 residues that undergo ubiquitination and SUMOylation are conserved

Three-dimensional structure of NcPCNA

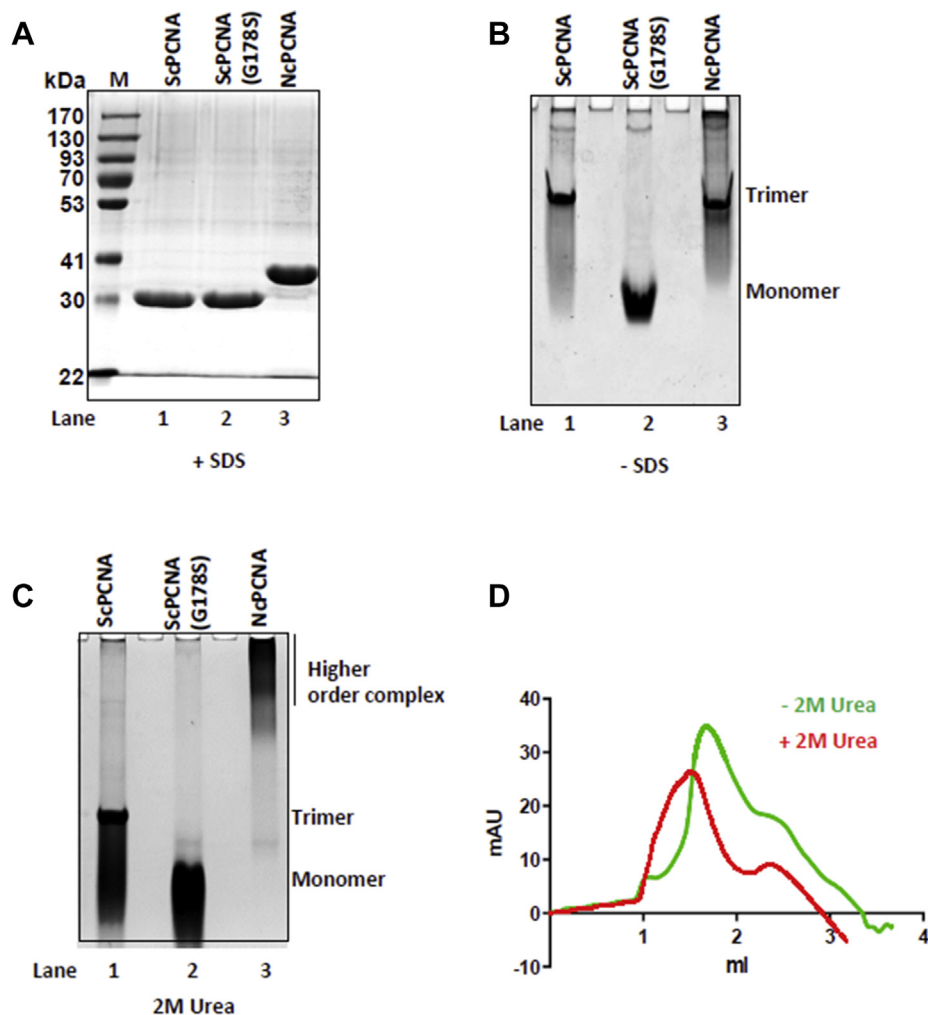


Figure 2. Purification and biochemical analysis of PCNAs. The WT and mutant PCNAs were purified, and about 1 μ g of each protein was analyzed in SDS-12% polyacrylamide gel (A), in 12% nondenaturing polyacrylamide gel (B), and 2 M urea-containing polyacrylamide gel (C). Lanes 1, ScPCNA; 2, ScPCNA G178S; and 3, NcPCNA. D, size-exclusion chromatograms of NcPCNA upon resolving it in a buffer with 2 M urea (red) or without urea (green). NcPCNA, *N. crassa* PCNA; PCNA, proliferating cell nuclear antigen; ScPCNA, *S. cerevisiae* PCNA.

and are located at similar positions in their three-dimensional structures. Tyr114 and Tyr211 that undergo phosphorylation in human PCNA are also placed at similar positions in NcPCNA (Fig. S2C). Thus, the overall architecture of PCNA is conserved across fungal species. Because most of the residues that undergo epigenetic modifications are conserved in eukaryotic PCNAs, the modulation of PCNA functions by epigenetic modifications appears to be maintained during evolution.

Structural comparison of NcPCNA with group I and II fungal PCNA

Four major loops in a PCNA structure, such as the central loop (residues Asp41 to Ala46), J loop (residues Ser105 to Arg110), IDCL (residues Leu117 to Tyr133), and P loop (residues Gln184 to Ile195), have functional significance (Fig. 3D). These loops are reported to be involved in recruiting other binding partners directly or through epigenetic modifications.

While the IDCL, central, and P loops exhibit higher amino acid sequence homology across different organisms, the residues in the J loop of PCNAs show significant diversity (Fig. 1). Irrespective of sequence homology, the conformations of these loop regions are distinct among different species and could be responsible for species specificity. The IDCL, P loop, and J loop exhibit considerable flexibility and adopt different states (9). Usually, owing to high flexibility, IDCLs are unstructured in some of the protomers of the various available PCNA trimer structures. Interestingly, in the crystal structure of NcPCNA, the protomer revealed a stable IDCL structure. Upon overlapping with other fungal PCNA structures, we observed noticeable differences in the IDCL conformations (Fig. 4A and Fig. S3A). Only a partial overlapping of the IDCLs was observed. IDCL residues of group I PCNAs (Sc and Ca) are quite different from that of group II PCNAs (Nc and Af), and it could be the reason behind distinct conformations. Because the IDCL acts as a hotspot for protein–protein interactions, these differences may impact the binding affinity of PCNA for

Table 1
Data collection and refinement statistics

Parameter	NcPCNA
Data collection	
Beamline	RRCAT-PX BL21
Detector type	MAR mosaic 225 mm CCD
Wavelength (Å)	0.9794
Data collection temperature (K)	100
Space group	<i>H3</i>
a, b, c (Å)	86.29, 86.29, 91.94
α, β, γ (°)	90, 90, 120
Resolution (Å)	39.15–1.95 (2.0–1.95)
Mean $I/\sigma(I)$	12.5 (1.9)
$CC_{1/2}$	0.994 (0.602)
Completeness (%)	99.9 (100)
Total number of reflections	109,680 (7782)
$R_{p.i.m.}$	0.075 (0.541)
R_{merge}	0.105 (0.750)
R_{meas}	0.129 (0.928)
Multiplicity	5.9 (5.8)
Wilson B-factor (Å ²)	21.1
Matthew's coefficient (Å ³ /Da)	2.26
Solvent content (%)	45.63
No. of molecules in ASU	1
Refinement	
No. of unique reflections	18,622 (1336)
Twinning type/fraction	Merohedral/0.192
Twin law	h, -h-k, -l
R_{work}/R_{free} (%)	19.6/23.5
Total no. of atoms	2123
No. of protein atoms	1975
No. of solvent atoms	148
Mean B-factor (Å ²)	29.0
Mean B-factor main chain atoms (Å ²)	27.18
Mean B-factor side chain atoms (Å ²)	31.53
RMSD	
Bond lengths (Å)	0.01
Bond angles (°)	1.138
Ramachandran plot (%)	
Favored region	96.85
Allowed region	3.15
Outliers	0.0
Clash score	2.0
MolProbity score	1.23
PDB ID	7EP8

its interaction partners, thereby impacting PCNA functions in the cell.

Structural alignment of NcPCNA with CaPCNA, AfPCNA, and ScPCNA revealed distinct conformations in the J loop region among the fungal PCNAs (Fig. 4B). The position of the J loop of NcPCNA was found to be displaced 7 Å away from that of the J loop of ScPCNA (Fig. 4B and Fig. S3B). The P loop (residues Gln184 to Ile195) of PCNA is a *bona fide* site for epigenetic modifications such as SUMOylation and ubiquitination. There are no significant changes in this region between the different fungal PCNA structures (Fig. 4C). At the monomer–monomer interface, the antiparallel β -strands β_{13} and $\beta_{9'}$ are held by extensive hydrogen bonds. The residues involved and the bonding patterns between these β -strands are similar among the different fungal species (Fig. 4D, Table 2). However, the interface formed by the α -helices α_3 and $\alpha_{2'}$ showed some differences in NcPCNA. At this α -helical interface of NcPCNA, Lys77 does not form any hydrogen bond because of its different orientation (Fig. 4E). However, Lys77 forms a hydrogen bond with Ala153, Lys153, and Asn153 residue in AfPCNA, ScPCNA, and CaPCNA, respectively. Similarly, Arg146 makes another unique interaction in NcPCNA. Arg146 forms hydrogen bonds with Arg80 and Ala82 in NcPCNA. In the case of

AfPCNA, Glu146 interacts with Asn83, whereas in CaPCNA and ScPCNA, the corresponding Lys146 forms hydrogen bonds with Ser81 and Arg80, respectively. Another differential interaction mode is displayed by Glu143, where it interacts with Arg110 in both ScPCNA and AfPCNA. However, in NcPCNA, the Glu143 forms a hydrogen bond with Asn108 instead of the residue at position 110 (Fig. 4E). Thus, although the overall architecture of PCNA is conserved, structural alterations in the loops and interface exist among the fungal PCNAs that could attribute to stability and functional variations.

Differential interaction of ScPol32 and T2AA with ScPCNA and NcPCNA

We compared the binding affinities of NcPCNA and ScPCNA with Pol32, the PCNA-binding subunit of replicative DNA polymerase delta and T2-amino alcohol (T2AA) that has been shown to interact with human PCNA by isothermal titration calorimetry (ITC). T2AA was identified as a small-molecule inhibitor of human PCNA, which interacts in the hydrophobic pocket and precludes p²¹ binding. Both PIPs of ScPol32 and T2AA were shown to interact with the hydrophobic pocket formed by the IDCL of PCNA. Although the IDCL sequences vary between NcPCNA and ScPCNA, the PIP sequences of the Pol32 subunit are remarkably identical in fungi and represent a canonical PIP box motif (Fig. S1B). Interestingly, ScPol32 binds to both ScPCNA and NcPCNA with about equal binding affinity. Our ITC analyses revealed exothermic binding kinetics for the interaction of ScPol32 with both ScPCNA and NcPCNA with 1:1 stoichiometry for the PCNA monomers and the dissociation constant K_D in the micromolar range (~ 3 – 4 μ M) (Fig. 5, A and B, Table 3). Thus, it appears that the conformational differences in the IDCLs of ScPCNA and NcPCNA have no significant effect on binding, at least with ScPol32. Surprisingly, when we used T2AA as a ligand, we could observe different binding kinetics for ScPCNA and NcPCNA, suggesting the existence of structural differences in the hydrophobic pocket formed by their IDCLs. Here also, we observed an exothermic reaction when T2AA binds to NcPCNA; however, no significant change in the heat was observed when the same molecule was injected into the cell containing ScPCNA (Fig. 5, C and D, Table 3). T2AA interacted to a NcPCNA monomer in 1:1 stoichiometry ($N = 1$), and the kinetic parameters were determined as $\Delta H = -13.2$ kcal/mol, $\Delta G = -6.3$ kcal/mol, and $K_D = 8.4$ μ M (Fig. 5C). Despite our repeated efforts with varying concentrations of ScPCNA and T2AA, no significant heat exchange was observed, suggesting a weak or undetectable interaction between ScPCNA and T2AA. In our earlier study, we had observed that while human PCNA interacts quite strongly with T2AA, CaPCNA failed to show such binding, suggesting that T2AA has a higher affinity for group II PCNA than for group I PCNA (9). Although T2AA binds to NcPCNA, it does not inhibit NcPCNA functions in yeast cells, probably because of its lower affinity (μ M) than the human PCNA (nM) (Fig. S4A). Nevertheless, this study suggests that although the IDCL structures look similar, minor differences in the structure due

Three-dimensional structure of NcPCNA

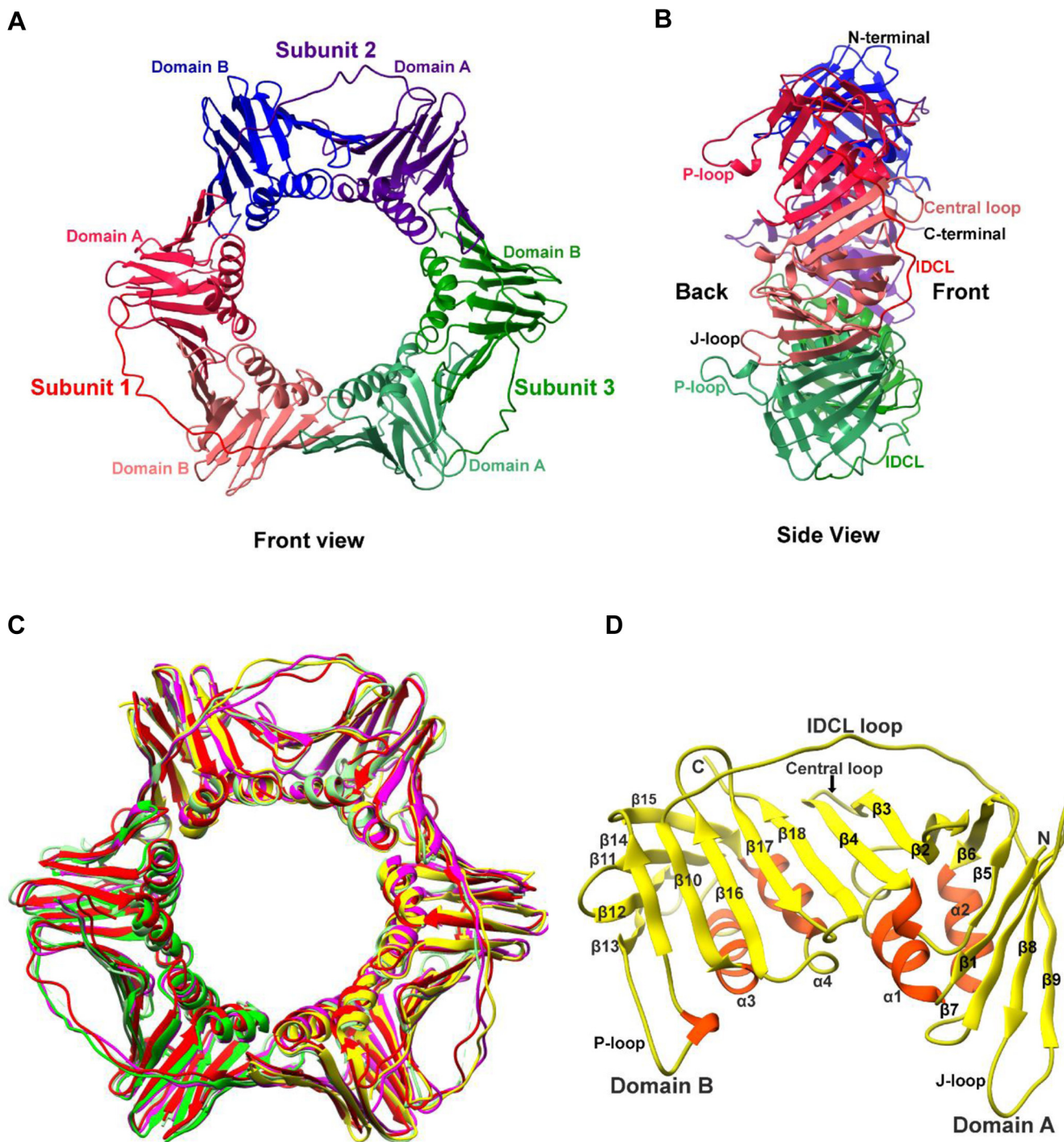


Figure 3. Structural features of *Neurospora crassa* PCNA. A, the crystal structure of NcPCNA homotrimeric ring in cartoon representation, illustrating the front face of PCNA with the three subunits 1, 2, and 3 (colored in shades of red, blue, and green, respectively). Domain A and domain B are marked. B, the side view of the NcPCNA, wherein the central loop, IDCL, P loop, and J loop are labeled. C, the overlapping three-dimensional structures of NcPCNA (purple, PDB ID: 7EP8), with ScPCNA (red, PDB ID: 4YHR), CaPCNA (green, PDB ID: 7BUP), and AfPCNA (yellow, PDB ID: STUP). D, the structural features of an individual subunit of NcPCNA, wherein the secondary structural elements are numbered, and domain A, domain B, and the important loops are labeled. AfPCNA, *A. fumigatus* PCNA; CaPCNA, *C. albicans* PCNA; IDCL, interdomain connecting loop; NcPCNA, *N. crassa* PCNA; PCNA, proliferating cell nuclear antigen; ScPCNA, *S. cerevisiae* PCNA.

to sequence variations in IDCLs play a significant role in determining the affinity of various ligands binding to IDCL. T2AA binding into the hydrophobic cavity of human PCNA (HsPCNA) (PDB ID: 3WGW) revealed that His44, Glu124, and Gln131 residues stabilize T2AA via hydrogen bonds and

other residues such as Met40 and Tyr250 interact with T2AA via hydrophobic interactions (Fig. S4, B and C). Most of these residues are conserved in fungal PCNAs except Gln131 residue. Additional structural analysis suggested that the hydrophobic pockets of group I PCNAs showed shallow or

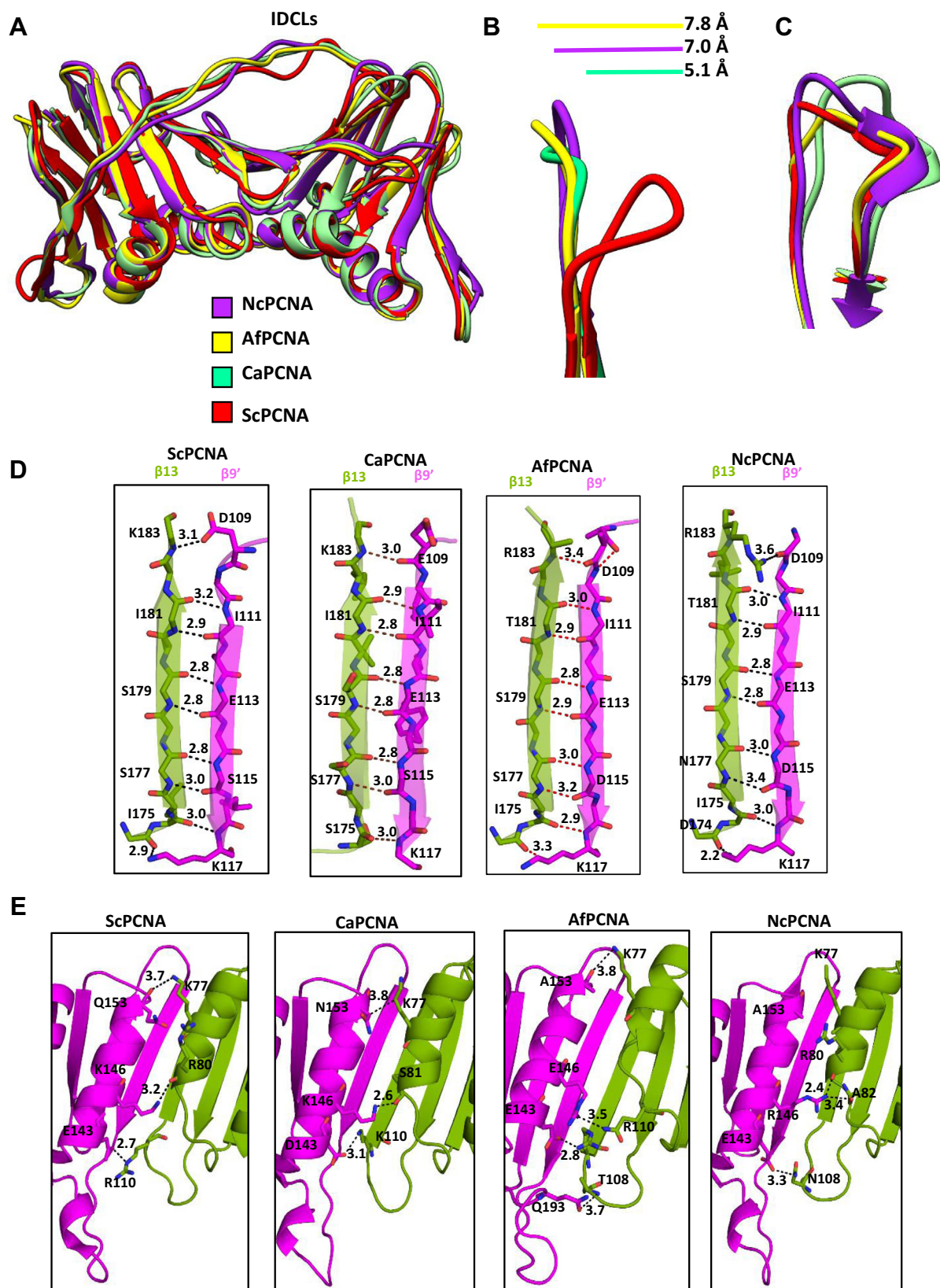


Figure 4. Comparison of NcPCNA monomer structure with other PCNA structures. *A*, structural alignment of PCNA monomers from different organisms in cartoon representation. IDCL exhibits minimum overlapping among PCNAs. *B*, structural alignment of the J loop from various fungal PCNAs. *C*, structural alignment of the P loop from various fungal PCNAs such as NcPCNA (purple), AfPCNA (yellow), CaPCNA (green), and ScPCNA (red). *D*, the monomer-monomer interface of fungal PCNAs as indicated in cartoon and stick representations, showing the intersubunit interactions mediated through the anti-parallel β -strands $\beta 13$ and $\beta 9'$. The hydrogen bonds are labeled as dashed lines, along with the respective bond lengths in Å. *E*, the monomer-monomer interface of fungal PCNAs, showing the intersubunit interactions mediated through the α helices $\alpha 3$ and $\alpha 2'$, in cartoon as well as stick representations. The hydrogen bonds and salt bridge are shown as dashed lines and the respective bond lengths in Å. AfPCNA, *A. fumigatus* PCNA; CaPCNA, *C. albicans* PCNA; IDCL, interdomain connecting loop; NcPCNA, *N. crassa* PCNA; PCNA, proliferating cell nuclear antigen; ScPCNA, *S. cerevisiae* PCNA.

Three-dimensional structure of NcPCNA

Table 2
Hydrogen bonds at the subunit interface

Species	Hydrogen bonds	Bond length (Å)
<i>Neurospora crassa</i>	Main chain-main chain	
	Asp109 [O]... Arg183 [NH1]	3.60
	Ile111 [N]...Thr181 [O]	3.04
	Ile111 [O]...Thr181 [N]	2.90
	Glu113 [N]...Ser179 [O]	2.81
	Glu113 [O]...Ser179 [N]	2.84
	Asp115 [N]...Asn177 [O]	3.01
	Asp115 [O]...Asn177 [N]	3.43
	Lys117 [N]...Ile175 [O]	2.99
	Main chain-side chain	
	Arg80 [O]...Arg146 [NH ₂]	2.40
	Ala82 [O]... Arg146 [NH ₂]	3.40
	Asn108 [ND2]...Glu143 [OE2]	3.30
	Lys117 [NZ]...Asp174 [O]	2.20
	Salt bridge	
	-Not observed-	

bifurcated cavities than group II, which may cause steric hindrance to T2AA binding (Fig. S5).

NcPCNA complements the essential function of POL30 in *S. cerevisiae*

POL30 gene that encodes for PCNA is essential for cell survival. To examine the ability of NcPCNA to complement ScPCNA, plasmid segregation was carried out using plasmid bumping and 5-fluoroorotic acid (5-FOA) counter-selection assays in two different strains of *S. cerevisiae* as described earlier (6). In one approach, the resident ScPCNA plasmid with selection marker *TRP1* was attempted to be replaced by an incoming plasmid without or with expressing NcPCNA having nutritional marker *URA3* in YTS9 strain by selectively growing only in synthetic defined (SD) media lacking uracil for several generations. Retention of both the auxotrophic markers despite selection pressure indicates the inability of the incoming plasmid to cure the original plasmid, thereby lack of complementation by the tester plasmid. As depicted in Figure 6A, colonies containing NcPCNA and WT ScPCNA could replace the resident plasmid (Fig. 6A sectors 1 and 2, and 3 and 4), and about 100% efficient curing was achieved. As expected, growth of the colonies harboring the vector alone in sectors 5 and 6 on both the plates suggested noncuring of the resident plasmid.

In another approach, various PCNA constructs were transformed into a YNA11 yeast strain that lacks the chromosomal *POL30* gene, but the cell viability is maintained by 2 μ -ADH1p-ScPCNA-URA3-based plasmid to allow positive as well as a counter selection of this plasmid by 5-fluoroorotic acid (5-FOA). The classical plasmid curing by selectively growing on media lacking leucine and 5-FOA counter selection strategies were used to study complementation analysis. Similar to in Figure 6A, while the transformants with any WT PCNAs could replace the resident plasmid for cell survival, the vector alone could not remove it in the YNA11 strain (Fig. 6B, compare sectors 1–4 with 5 and 6). Furthermore, the 5-FOA sensitivity assays also confirmed that the cells harboring NcPCNA or ScPCNA, but not the vector control, could grow on 5-FOA-containing SD medium, in which the resident plasmid (*URA3*) was negatively selected (Fig. 6C, compare sector 1 with sectors 2

and 3). Cytotoxicity by 5-FOA is due to the retention of the *URA3* gene in a strain. Taken together, we conclude that NcPCNA can complement the essential functions of yeast *POL30* and supports cell viability.

Phenotypes of *S. cerevisiae* bearing NcPCNA under genotoxic stress

Several ScPCNA mutants have been characterized that support cell viability but are inefficient in DNA replication and repair. Therefore, *S. cerevisiae* bearing such PCNA mutants display slow growth phenotype and sensitivity to genotoxic agents (15). To characterize NcPCNA further, growth rates of *S. cerevisiae* strains expressing PCNAs in low or high copy number plasmids were monitored. As shown in Figure 7A, strains harboring NcPCNA displayed intermediate growth rates between YTS9 (ScPCNA D41A, D42A) and the strains harboring ScPCNA. High copy number expression of NcPCNA in *S. cerevisiae* did not result in any significant growth advantage over the low copy number plasmid-based expression. Thus, the slow growth phenotype of NcPCNA could be because of inefficient DNA replication in *S. cerevisiae*. To confirm that the slow growth defects of various yeast strains are not due to the differences in the expression levels of PCNAs and are rather due to the intrinsic properties of NcPCNA, RT-PCR was carried out. Our results suggested no noticeable difference in the expression levels of NcPCNA and ScPCNA while expressed under the *ADH1* promoter (data not shown).

To understand the role of NcPCNA in DNA replication and repair, the susceptibility of *S. cerevisiae* bearing NcPCNA to hydroxyurea (HU), methyl methanesulfonate (MMS), H₂O₂, and UV was investigated (Fig. 7B). While HU has been widely used as a replication inhibitor that depletes cellular dNTPs pool, MMS, H₂O₂, and UV directly attack genomic DNA and generate various DNA lesions. To our surprise, the yeast strain possessing NcPCNA showed severe growth retardation under genotoxic stress similar to the strain having ScPCNA with D41A, D42A mutations. Yeast strain expressing heterologous NcPCNA or ScPCNA with D41A, D42A mutations displayed cytotoxicity in 12.5 mM HU, 0.0012% MMS, 0.04% H₂O₂, and 6 J/m² of UV stresses (Fig. 7B compare rows 1 and 3 with 2). Yeast strain expressing ScPCNA was resistant to the genotoxins mentioned above. Thus, our results suggested that NcPCNA is relatively less efficient in coordinating DNA replication and repair processes in *S. cerevisiae*.

NcPCNA mutants mimicking IDCL and J loop of ScPCNA function efficiently in *S. cerevisiae*

Our analyses suggested that the structure of NcPCNA differs mostly in the IDCL and J loop regions compared with ScPCNA. Interestingly, NcPCNA and CaPCNA are structurally more related in these regions than ScPCNA, and both Nc- and Ca-PCNAs function inefficiently in *S. cerevisiae*. Second, we noticed four key residues each that showed minimal conservation between NcPCNA and ScPCNA in the IDCL and J loop. The residues A123, F125, K127, and E129 in the IDCL

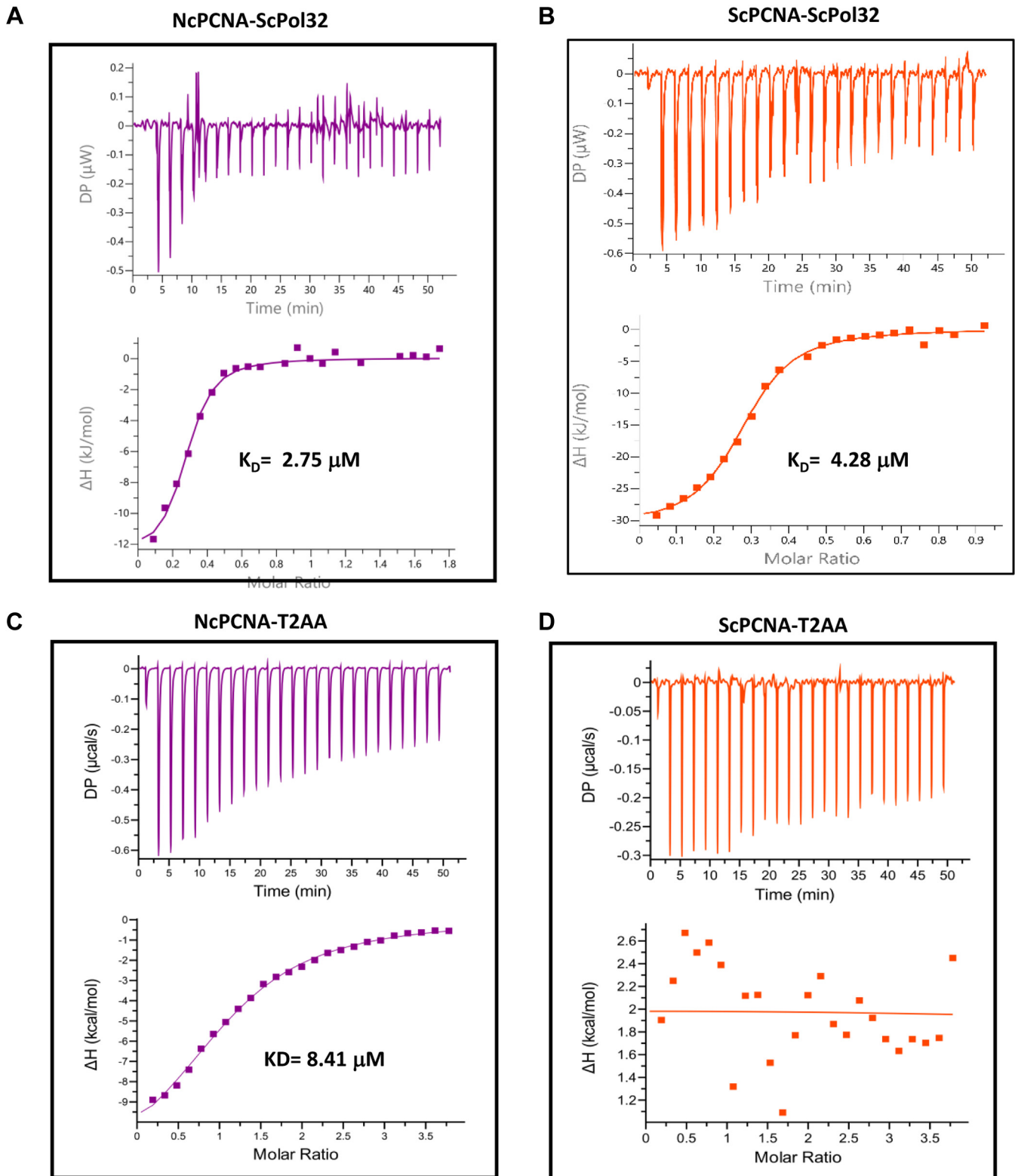


Figure 5. Binding of Pol32 protein and T2AA small molecule to PCNA by ITC analysis. ITC analyses of the binding of the PCNAs with the ligands: (A) NcPCNA with ScPol32; (B) ScPCNA with ScPol32; (C) NcPCNA with T2AA; (D) ScPCNA with T2AA. In each subfigure, the *upper panel* shows the measured heat exchanges during the injection of each inhibitor. The *lower panel* of each subfigure shows the enthalpy changes as a function of the molar ratio of inhibitors to a PCNA monomer. *Squares and lines* denote the raw measurements and the fitting to one set of identical sites mode, respectively. ITC, isothermal titration calorimetry; NcPCNA, *N. crassa* PCNA; PCNA, proliferating cell nuclear antigen; ScPCNA, *S. cerevisiae* PCNA; T2AA, T2-amino alcohol hydrochloride.

Three-dimensional structure of NcPCNA

Table 3
Binding kinetic parameters as determined by isothermal titration calorimetry

Protein	Ligand	K_D	N (site)	ΔH (KJ mol ⁻¹)	$-T\Delta S$ (KJ mol ⁻¹)	ΔG (KJ mol ⁻¹)
ScPCNA	ScPol32	2.75 μ M \pm 0.430	1.05 \pm 0.017	-6.18 \pm 0.185	-25.6	-31.8
NcPCNA	ScPol32	4.28 μ M \pm 0.325	1.06 \pm 0.035	-5.17 \pm 0.232	-26	-31.7
ScPCNA	T2AA	NA	NA	NA	NA	NA
NcPCNA	T2AA	8.41 μ M \pm 0.558	1.08 \pm 0.026	-13.2 \pm 0.435	6.24	-6.93

Abbreviation: NA, not applicable.

and the residues D105, T106, K107, and K108 in the J loop of ScPCNA are evolutionarily replaced by Q123, H125, G127, and P129 and S105, S106, E107, and N108 in NcPCNA, respectively (Fig. 1A and Fig. S1A). Therefore, to understand the implication of random variations in these key loops of PCNA, we generated four NcPCNA mutants that would mimic IDCL and J loop of ScPCNA. PCNA mutants NcPCNA-IDCL1 (Q123A, G127K, and P129E), NcPCNA-IDCL2 (Q123A, H125F, G127K, and P129E), NcPCNA-J loop (S105D, S106T, E107K, and N108K), and NcPCNA-IDCL2-J loop (S105D, S106T, E107K, N108K, Q123A, H125F, G127K, and P129E) were expressed under *S. cerevisiae* ADHI constitutive promoter, and their ability to support viability of *S. cerevisiae* strain was determined (Fig. 6C). 5-FOA sensitivity suggested that both the IDCL and J loop variants supported the growth of *S. cerevisiae* pol30 Δ strain similar to WT NcPCNA and ScPCNA; however, the vector control strain did not grow on 5-FOA-containing SD medium, in which the resident plasmid (*URA3*) was negatively selected (Fig. 6C, compare sector 1 with sectors 2–7). When these strains were exposed to genotoxic stress, we found that yeast strains possessing the NcPCNA variants showed considerably improved tolerance to HU, MMS, H₂O₂, and UV in comparison with the yeast strain expressing WT NcPCNA or D41A, D42A mutant of ScPCNA (Fig. 7B compare rows 1 and 3 with rows 4–7). Except in MMS treatment, both the IDCL and J loop variants of NcPCNA possessing yeast cells exhibited similar tolerance like ScPCNA. At a higher concentration of MMS, yeast cells expressing NcPCNA with IDCL1 or J loop mutations conferred similar cellular sensitivity as WT NcPCNA (Fig. 7B III, rows 3, 4, and 6). The NcPCNA-IDCL2 mutant possesses an additional mutation H125F and confers better tolerance to genotoxic agents than the IDCL1 mutant. This suggests that the presence of an additional hydrophobic residue Phe in the hydrophobic pocket of PCNA could be stabilizing the interaction with PCNA-binding proteins. To confirm these results, we estimated the number of survived colonies after exposure to different genotoxic agents (Fig. 7, C–E). The *S. cerevisiae* cells expressing WT ScPCNA or NcPCNA with both IDCL2 and J loop mutations formed an equal number of colonies upon treatment with genotoxins and were growing better than cells expressing either WT NcPCNA or with mutations in either IDCL or J loop. Interestingly, *S. cerevisiae* cells harboring D41A, D42A ScPCNA mutants developed more colonies on each treated plate than the cells expressing WT NcPCNA. Taken together, our results suggested that although IDCL sequence conservation is important for PCNA functions, it is not solely responsible for its efficient function in replication and repair.

Other interaction zones, such as the J loop, could also play an equally critical role in PCNA functioning in the cell. Because the J loop has been shown to functionally interact with TLS DNA polymerases, mimicking this region of NcPCNA with that of ScPCNA might facilitate stronger interaction than WT NcPCNA with DNA polymerases of *S. cerevisiae* involved in DNA damage response pathways. Thus, both IDCL and J loop determine species specificity of PCNA.

Discussion

The three-dimensional structure of a protein is directly correlated to its function, and remarkably, the structure is determined by its amino acid composition. Despite little amino acid similarities, PCNA structures are extraordinarily similar across eukaryotic organisms. So how does PCNA maintain its species specificity? The way PCNA from *S. cerevisiae* folds into a toroidal-shaped structure, PCNA from humans also forms a similar structure (7, 8). Interestingly, the amino acid sequence similarity is barely less than 35% between these two PCNAs (15). Despite the structural conservation between ScPCNA and HsPCNA, HsPCNA does not complement the loss of PCNA function in *S. cerevisiae* and *vice versa* because of its inability to interact with host cellular proteins (15, 16). *In vitro* stimulation of DNA polymerase activities by PCNAs from various heterologous sources has been carried out in the past by several groups (16–18). These reports, however, do not reflect PCNA function in the cellular context as cross-species compatibility of PCNAs rarely exists. Therefore, to understand species specificity, in this study, we have explored the function of PCNA from *N. crassa* and included our earlier observations from PCNA of *C. albicans* (6, 9), two closely related fungal species of *S. cerevisiae*, where the PCNA-interacting protein network is expected to be conserved. We found that the species specificity of PCNA is intrinsic to its structure, and the two structural elements IDCL and J loop are central to its function in a given species.

Based on sequence similarity in IDCL sequence, PCNA from *S. cerevisiae* and *C. albicans* were placed in group I complementation group (11). The IDCL is composed of 16 amino acid residues, and these residues are evolutionarily conserved in the group I PCNAs, but they have diverged in the group II PCNAs. Because PIP or PIP-like motifs of DNA polymerases or other interacting proteins bind to the hydrophobic pocket formed by the IDCL, it is expected that PCNA from the group I but not group II would be functional in *S. cerevisiae*. Accordingly, swapping of the IDCL of ScPCNA with the group I IDCLs had no apparent effect on ScPCNA

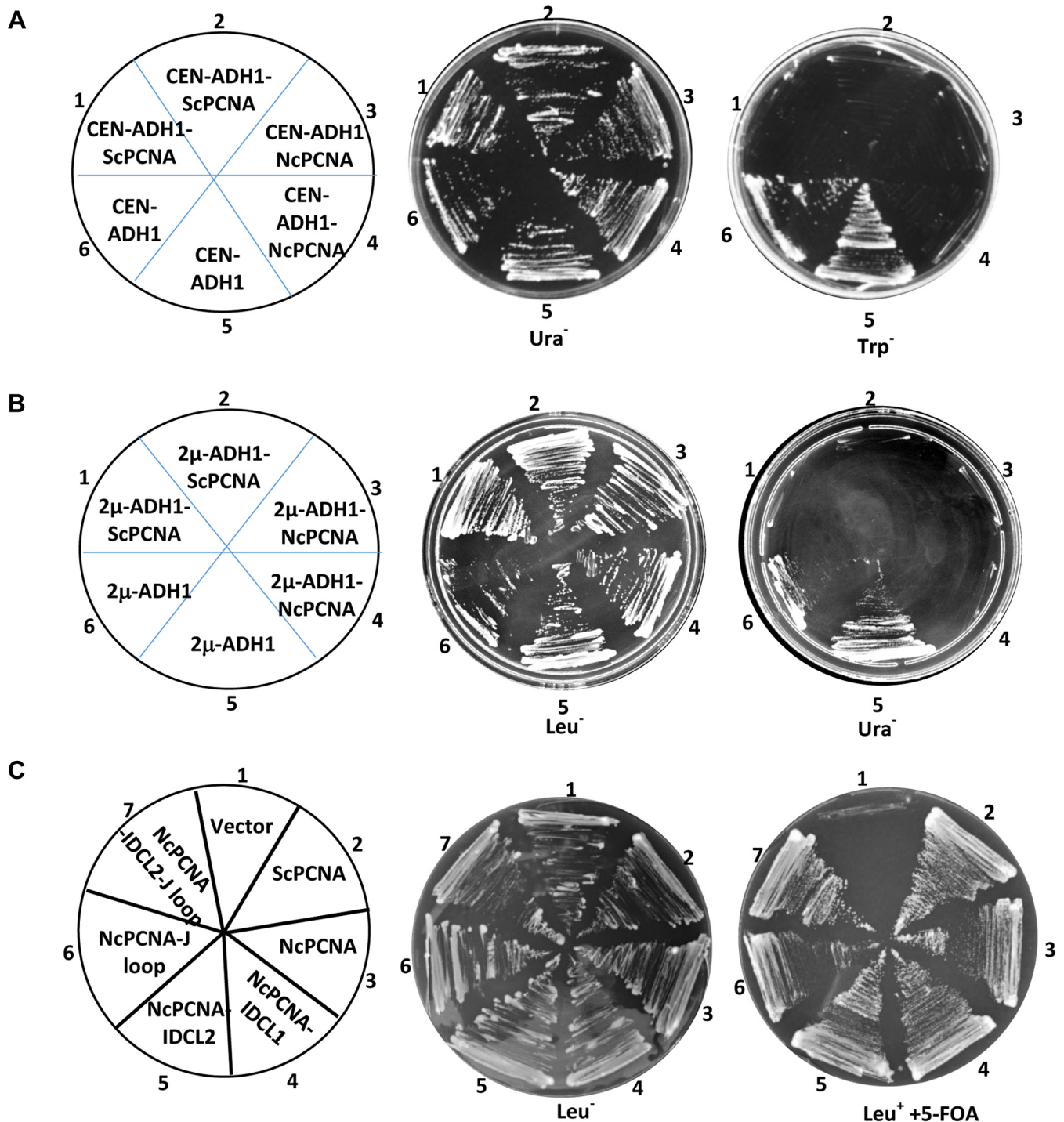


Figure 6. Complementation analysis of PCNAs. A, plasmid curing of YTS9 strain (trp^+ , ura^+) transformants containing various plasmids was carried out by selectively growing on synthetic media omitting uracil at $30^\circ C$ to cure the resident plasmid (trp^+) as described in [Experimental procedures](#). After seven consecutive subcultures, the possession of nutritional markers was tested by plating on SD agar plates lacking uracil alone or tryptophan alone. Plates were incubated for 2 days at $30^\circ C$ and photographed. Sectors 1 and 2, CEN, ADH1p-ScPCNA; sectors 3 and 4, CEN, ADH1p-NcPCNA; and sectors 5 and 6, CEN, ADH1p (empty vector). B, plasmid curing of YNA11 strains (leu^+ , ura^+) transformants containing various plasmids were carried out by selectively growing on synthetic media, omitting leucine at $30^\circ C$ to cure the resident plasmid (ura^+) as described in [Experimental procedures](#). After seven consecutive subcultures, the presence of the nutritional markers was tested by plating on SD agar plates lacking uracil alone or leucine alone. Plates were incubated for 2 days at $30^\circ C$ and photographed. Sectors 1 and 2, 2μ , ADH1p-ScPCNA, sectors 3 and 4, 2μ , ADH1p-NcPCNA, and sectors 5 and 6, 2μ , ADH1p (empty vector). C, the transformants of yeast strain YNA11 (ura^+) containing various plasmids were selected on SD media without leucine and uracil. Isolated colonies were picked and restreaked on SD-leucine plate but with or without 5-FOA. Plates were incubated for 2 days at $30^\circ C$ and photographed. Sector 1, 2μ , ADH1p (empty vector), sector 2, 2μ , ADH1p-ScPCNA, sector 3, 2μ , ADH1p-NcPCNA, sector 4, 2μ , ADH1p-NcPCNA IDCL1 (Q123A, G127K, and P129E), sector 5, 2μ , ADH1p-NcPCNA IDCL2 (Q123A, H125F, G127K, and P129E), sector 6, 2μ , ADH1p-NcPCNA J loop (S105D, S106T, E107K, and N108K), sector 7, 2μ , ADH1p-NcPCNA IDCL2-J loop (S105D, S106T, E107K, N108K, Q123A, H125F, G127K, and P129E). NcPCNA, *N. crassa* PCNA; PCNA, proliferating cell nuclear antigen; ScPCNA, *S. cerevisiae* PCNA; SD, synthetic defined.

Three-dimensional structure of NcPCNA

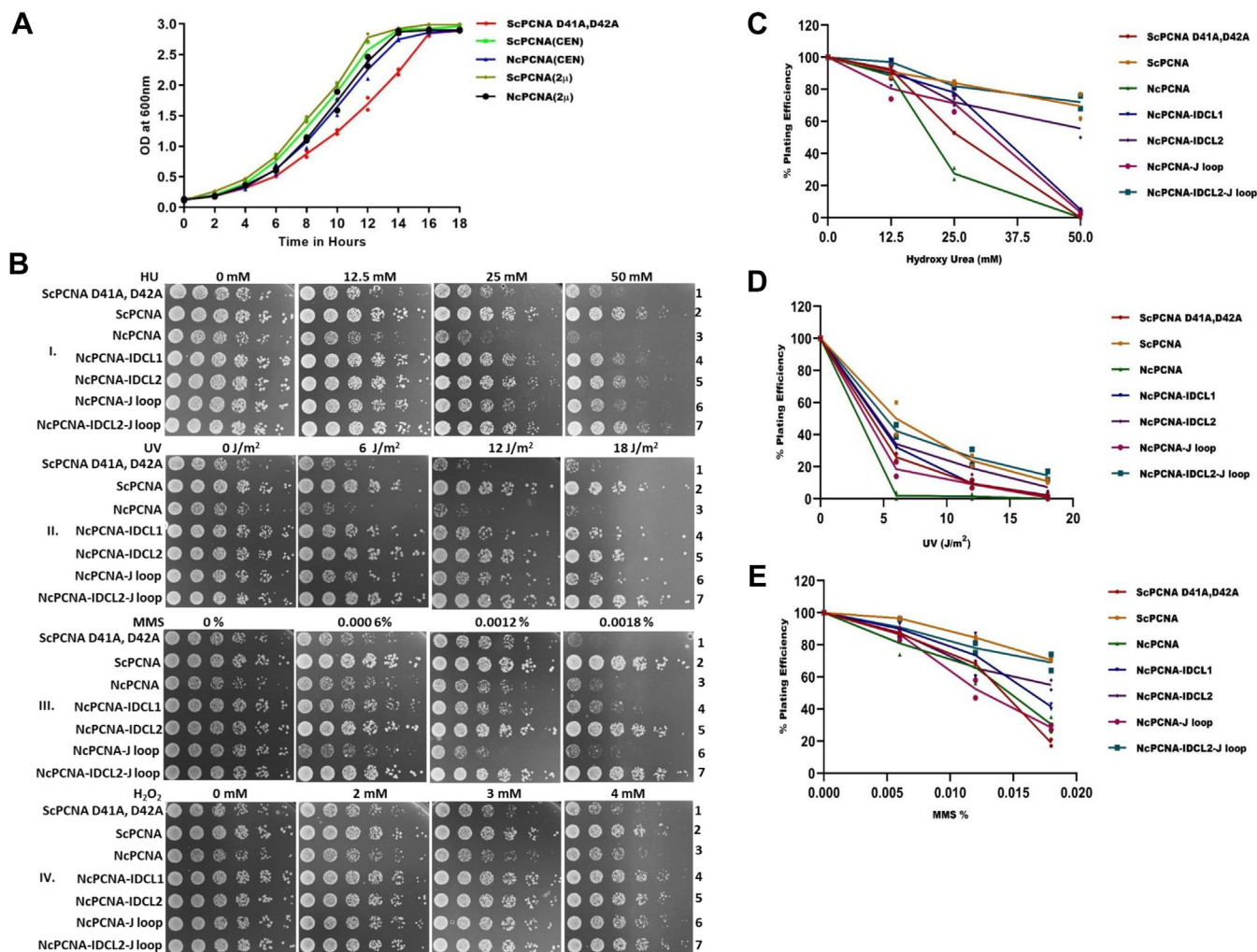


Figure 7. Phenotypes of yeast strain harboring NcPCNA. *A*, growth curves of various yeast strains expressing PCNA. D41A, D42A ScPCNA mutant (red), CEN-ADH1p-ScPCNA (green), 2 μ -ADH1p-ScPCNA (sea green), CEN-ADH1p-NcPCNA (blue), and 2 μ -ADH1p-NcPCNA (black) were grown in 100 ml YPD liquid medium at 30 °C, and absorbance at 600 nm was measured at regular intervals. The plot was an average of two set of experiments carried out in duplicates. *B*, overnight YPD culture of genomic *pol30 Δ* yeast strains containing WT or D41A, D42A mutants of ScPCNA or WT NcPCNA or NcPCNA-IDCL1 (Q123A, G127K, and P129E) or NcPCNA-IDCL2 (Q123A, H125F, G127K, and P129E) or NcPCNA-J loop (S105D, S106T, E107K, and N108K), or NcPCNA-IDCL2-J loop (S105D, S106T, E107K, N108K, Q123A, H125F, G127K, and P129E) mutants were serially diluted and spotted onto YPD plates without or with indicated concentrations of HU (I), MMS (III), and H₂O₂ (IV). For UV (II), spotted plates were exposed to the mentioned doses of UV radiation and covered with aluminum foil to prevent direct repair. Furthermore, the plates were incubated at 30 °C for 2 days and then photographed. For colony-forming unit analyses, logarithmically growing cells were diluted to about 500 cells/ml, from which 200 μ l was spread onto YPD plates without or with HU (C), UV (D), and MMS (E) treatment. The experiment was repeated twice with two experimental triplicates. HU, hydroxyurea; MMS, methyl methanesulfonate; NcPCNA, *N. crassa* PCNA; PCNA, proliferating cell nuclear antigen; ScPCNA, *S. cerevisiae* PCNA; YPD, yeast extract, peptone, dextrose.

function (11). However, IDCLs of the group II containing ScPCNAs are incapable of efficiently functioning in *S. cerevisiae*. For example, ScPCNA with IDCLs of CaPCNA was fully functional in *S. cerevisiae*. Simultaneously, the hybrid of ScPCNA with the IDCL from *S. pombe* PCNA (SpPCNA) was inefficient in DNA replication and repair, and thus, it only complemented partially. Yeast two-hybrid analyses further revealed that the chimeric ScPCNAs with IDCLs of group I could interact with *S. cerevisiae* proteins with about equal or better affinity. However, IDCLs of group II appeared incompatible with those group I, wherein they compromised in the binding affinity. Therefore, it was suggested that IDCL-partner interaction networks determine species-specific compatibility of PCNA and form functional barriers between fungal species. Contrarily, in our study, we found that

CaPCNA, unlike chimeric ScPCNA with IDCL of CaPCNA, partially complemented PCNA functions in *pol30 Δ* *S. cerevisiae* strain (6). The *pol30 Δ* *S. cerevisiae* strain harboring CaPCNA was more susceptible to genotoxic agents than the strain containing ScPCNA. To understand this phenomenon further, we determined the structure of CaPCNA by X-ray crystallography and SAXS. We found that the structure of the J loop of CaPCNA deviated 5.1 Å away from ScPCNA (9). A minor change in IDCL and P loop folding were also observed. So the cross-species incompatibility of CaPCNA could be because of J loop structural alterations. Variants of ScPCNA with altered J loop structure were shown to be functionally inefficient in *S. cerevisiae*. The structural analyses of ScPCNA with G178S or E113G mutations suggested that the J loop adopted a different conformation from that in WT ScPCNA.

When superimposed, the J loop of G178S, E113G ScPCNA mutants and CaPCNA deviated 6.5 Å, 3 Å, and 5.1 Å from the J loop structure of WT ScPCNA, respectively (Fig. S3). Biochemical analyses suggested that these two ScPCNA mutants inhibited translesion DNA synthesis by ScPol η and ScPol ζ , and cells harboring these PCNA mutants exhibited DNA damaging agent sensitivity and enhanced mutagenesis compared with WT (12, 13). Pol η and Pol ζ are specialized DNA polymerases involved in translesion DNA synthesis and damage tolerance pathways (19–21).

To further understand the role of the IDCL and J loop in species specificity, this study was designed to uncover the detailed structure of NcPCNA, a PCNA from the group II compatibility group, and its functional analyses in *S. cerevisiae*. The structure of PCNA from *A. fumigatus* has been determined, yet another PCNA from group II (10). However, its functional analysis is yet to be carried out. Our crystallographic analyses unraveled that the overall architecture of NcPCNA displayed a high degree of conservation with other eukaryotic PCNAs. It forms a stable homotrimer in the crystal structure, as determined by native PAGE and size-exclusion chromatography as well. Minor changes in the hydrogen-bonding patterns in the monomer–monomer interfaces of PCNAs do not appear to affect the stability of the trimers. The surface charge distribution, residues in the oligomeric interface, and the DNA-binding residues lining the central pore are also well conserved among the PCNA from different fungi. Interestingly, the structure of NcPCNA shows more resemblance with CaPCNA and AfPCNA than with ScPCNA. The IDCLs in these fungal PCNAs are rarely superimposed. We also observed a 7 Å deviation of the J loop of NcPCNA from that of ScPCNA when they were superimposed. Because of the overall similar architecture, NcPCNA supported the growth of an *S. cerevisiae* strain deficient in ScPCNA; however, like CaPCNA and ScPCNA mutants, NcPCNA was inefficient in carrying out DNA replication and repair in *S. cerevisiae* as cells harboring NcPCNA exhibited DNA damaging agent sensitivity compared with ScPCNA. Contrary to our finding, Zamir *et al.* (11) reported that NcPCNA or chimeric ScPCNA with the IDCL of NcPCNA, but not SpPCNA, did not support the growth of *pol30* Δ *S. cerevisiae* strain. SpPCNA also belongs to the group II compatibility group. Although we do not understand the exact reason behind NcPCNA not supporting the essential DNA replication function and viability of *pol30* Δ *S. cerevisiae* strain in their study, here we have used several constructs expressing both WT and variant forms of NcPCNA and have consistently shown that the yeast cells harboring NcPCNA are viable. Because NcPCNA harboring yeast cells showed sensitivity to genotoxins, we further explored the significance of divergence of amino acids in the IDCL and J loop.

NcPCNA exhibited variations of four key residues both in the IDCL and J loop, which could have implications in regulating the fungal-specific protein–protein interaction and function (Fig. 1A). Unlike the J loop, the structural difference was not apparent in the IDCLs. However, our ITC analyses revealed differential binding affinity of T2AA with

the PCNAs, suggesting significantly altered conformations exist among the IDCL structures. Our mutational analyses further suggested that NcPCNA with IDCL or J loop substitutions of ScPCNA residues was functional and efficiently carried out replication and repair functions better than the WT NcPCNA and D41A, D42A mutant of ScPCNA. Furthermore, the spot and colony-forming unit analyses clearly suggested that NcPCNA having both IDCL and J loop substitutions offered additional benefits to PCNA, and thereby, it functions as good as the WT ScPCNA. Thus, it suggested that while the overall architecture of a heterologous PCNA is critical for supporting viability and growth, both IDCL and J loop structures determine the efficient functioning of PCNA in a heterologous system. Whether these amino acid substitutions in the IDCL or J loop lead to regaining a PCNA structure similar to ScPCNA requires further investigation. Nevertheless, this study determined the importance of amino acid variation in the hydrophobic pocket and J loop of PCNA as the main functional barriers for species specificity. However, in distantly related species, the PCNA–protein network could also be a functional barrier for compatibility. Thus, the grouping of PCNAs based on the hydrophobic cavity sequence is redundant as PCNA is a highly species-specific protein despite similar overall structural architecture. This study has helped us understand the details of the complex interplay of binding between PCNA and its partner proteins in cells and the significance of amino acid sequence microdivergence in two critical loops of PCNA involved in the interaction. Because of the species specificity, we speculate that any therapeutic developments targeting PCNA will also be highly specific to that particular species.

Experimental procedures

Oligonucleotides, strains, and media

The oligonucleotides used in this study were procured from either Integrated DNA Technologies or Eurofins Genomics, India. *S. cerevisiae* EMY74.7 and *N. crassa* 74-OR23-1A were used as WT strains (22, 23). A protease-deficient yeast strain YRP654 was used to express ScPol32. YTS9, a *POL30* genomic null yeast strain supported by a YCplac22 (CEN, *TRP1*) plasmid-derived *POL30* with D41A, D42A mutations, was used for plasmid segregation analysis. Various yeast strains obtained by transforming different PCNA constructs to YTS9 and others used in this study are described in Table 4. The yeast strains were grown on yeast extract, peptone, dextrose (YPD) media with or without DNA-damaging agents or various synthetic drop-out media as required.

Multiple sequence alignment

Multiple sequence alignment of amino acid sequences of PCNA from *N. crassa* (UniProtKB-Q7SF71), *A. fumigatus* (UniProtKB-A0A0J5SJF1), *C. albicans* (UniProtKB-Q6FWA4), and *S. cerevisiae* (UniProtKB-P15873) was performed using the T-Coffee web server (24), and the resulting alignment was rendered through ESPript (25).

Three-dimensional structure of NcPCNA

Table 4
List of *Saccharomyces cerevisiae* strains used in the study

Strain	Genotype	Source/ reference
YTS09	<i>MATa ura3-52 trp1D901 leu2-3,112 can1 pol30Δ1</i> , with pBL230-6 (YCP50, TRP1, POL30 with DD41, 42AA)	(15)
YNA11	<i>MATa ura3-52 trp1D901 leu2-3,112 can1 pol30Δ1</i> , pNA1012 (2μ, ADH1p-ScPCNA, URA3)	(6)
YNA27	<i>MATa ura3-52 trp1D901 leu2-3,112 can1 pol30Δ1</i> , pNA1012 (2μ, ADH1p-ScPCNA, URA3), pNA745 (YEplac181, LEU2)	(6)
YNA35	<i>MATa ura3-52 trp1D901 leu2-3,112 can1 pol30Δ1</i> , pNA1012 (2μ, ADH1p-ScPCNA, URA3), pNA1190 (2μ, ADH1p-ScPCNA, LEU2)	(6)
YNA81	<i>MATa ura3-52 trp1D901 leu2-3,112 can1 pol30Δ1</i> , with pBL230-6 (YCP50, TRP1, POL30 with DD41, 42AA), pNA745 (YEplac181, LEU2)	This study
YNA85	<i>MATa ura3-52 trp1D901 leu2-3,112 can1 pol30Δ1</i> , pNA1012 (2μ, ADH1p-ScPCNA, URA3), pNA1623 (2μ, ADH1p-NcPCNA, LEU2)	This study
YNA86	<i>MATa ura3-52 trp1D901 leu2-3,112 can1 pol30Δ1</i> , pNA1623 (2μ, ADH1p-NcPCNA, LEU2)	This study
YNA87	<i>MATa ura3-52 trp1D901 leu2-3,112 can1 pol30Δ1</i> , pNA1190 (2μ, ADH1p-ScPCNA, LEU2)	This study
YNA113	<i>MATa ura3-52 trp1D901 leu2-3,112 can1 pol30Δ1</i> , with pBL230-6 (YCP50, TRP1, POL30 with DD41, 42AA), pNA1645 (CEN, ADH1p-ScPCNA, URA3).	This study
YNA114	<i>MATa ura3-52 trp1D901 leu2-3,112 can1 pol30Δ1</i> , pNA1645 (CEN, ADH1p-ScPCNA, URA3).	This study
YNA115	<i>MATa ura3-52 trp1D901 leu2-3,112 can1 pol30Δ1</i> , with pBL230-6 (YCP50, TRP1, POL30 with DD41, 42AA), pNA1646 (CEN, ADH1p-NcPCNA, URA3).	This study
YNA116	<i>MATa ura3-52 trp1D901 leu2-3,112 can1 pol30Δ1</i> , pNA1646 (CEN, ADH1p-NcPCNA, URA3).	This study
YNA117	<i>MATa ura3-52 trp1D901 leu2-3,112 can1 pol30Δ1</i> , with pBL230-6 (YCP50, TRP1, POL30 with DD41, 42AA), pNA742 (Ycplac33, URA3)	This study
YNA118	<i>MATa ura3-52 trp1D901 leu2-3,112 can1 pol30Δ1</i> , pNA1012 (2μ, ADH1p-ScPCNA, URA3), pNA1736 (2μ, ADH1p-NcPCNA IDCL1, LEU2)	This study
YNA119	<i>MATa ura3-52 trp1D901 leu2-3,112 can1 pol30Δ1</i> , pNA1736 (2μ, ADH1p-NcPCNA IDCL1, LEU2)	This study
YNA120	<i>MATa ura3-52 trp1D901 leu2-3,112 can1 pol30Δ1</i> , pNA1012 (2μ, ADH1p-ScPCNA, URA3), pNA1737 (2μ, ADH1p-NcPCNA IDCL2, LEU2)	This study
YNA121	<i>MATa ura3-52 trp1D901 leu2-3,112 can1 pol30Δ1</i> , pNA1737 (2μ, ADH1p-NcPCNA IDCL2, LEU2)	This study
YNA122	<i>MATa ura3-52 trp1D901 leu2-3,112 can1 pol30Δ1</i> , pNA1012 (2μ, ADH1p-ScPCNA, URA3), pNA1776 (2μ, ADH1p-NcPCNA J Loop, LEU2)	This study
YNA123	<i>MATa ura3-52 trp1D901 leu2-3,112 can1 pol30Δ1</i> , pNA1776 (2μ, ADH1p-NcPCNA J Loop, LEU2)	This study
YNA124	<i>MATa ura3-52 trp1D901 leu2-3,112 can1 pol30Δ1</i> , pNA1012 (2μ, ADH1p-ScPCNA, URA3), pNA1774 (2μ, ADH1p-NcPCNA J Loop IDCL2, LEU2)	This study
YNA125	<i>MATa ura3-52 trp1D901 leu2-3,112 can1 pol30Δ1</i> , pNA1774 (2μ, ADH1p-NcPCNA J Loop IDCL2, LEU2)	This study

Generation of PCNA constructs

NcPCNA ORF was amplified in a 50-μl PCR mixture containing 100 ng of cDNA, 200 μM dNTPs, 1 × Q5 reaction buffer with optimal Mg²⁺ concentration, 1 U of Q5 high-fidelity DNA polymerase (NEB), and 0.5 μM NAP436 (5'-GGC CGG ATC CAC ATA TGC TTG AAG CAC GGT TG-3') and NAP437 (5'-GGC CGG ATC CTT ACT CCT CGT CGC CAA TCT TG-3') primers. PCR conditions included initial heating at 98 °C for 1 min followed by 34 cycles at 98 °C for 30 s, 48 °C for 45 s, and 72 °C for 1 min. Amplified PCR product (~800 bp) was purified, digested with BamHI, and cloned into the same site of pUC19. The sequence of the cloned PCNA ORF was validated by DNA sequencing

using an in-house Applied Biosystems 3500 Series Genetic Analyzer. The BamHI fragment containing the NcPCNA ORF was further subcloned into the BglII site of a pGEX-6P-1 vector for bacterial expression with an amino-terminal GST-tag for protein expression and into the BamHI site of a vector to express in *S. cerevisiae* under the *ADH1* promoter. For protein crystallization, NcPCNA was PCR-amplified using NAP436 as the forward and NAP539 (5'-CCGG CTC GAG CTC CTC GTC GCC-3') as reverse primers, and the amplified PCR product was digested with NdeI-XhoI and cloned into a pET22b(+) vector for expression of the protein with an uncleavable hexahistidine tag at the C terminus.

Site-directed mutagenesis

Two NcPCNA variants (NcPCNA-IDCL1 harboring Q123A, G127K, and P129E mutations and NcPCNA-IDCL2 harboring Q123A, H125F, G127K, and P129E mutations) were generated to make the IDCL of NcPCNA mimicking ScPCNA. An amino-terminal fragment of NcPCNA was amplified using similar PCR conditions as above but with M13 forward primer that anneals to the sequence upstream to the HindIII site of pUC19 and a reverse primer NAP613 (5'-AGA CGG CAT GCT GAT GGT GGC CGC GTA CTC GGT ATC CTC AAT CTT CAG GTG CTC CGC GTC AAT G-3') or NAP614 (5'-AGA CGG CAT GCT GAT GGT GGC CGC GTA CTC GGT ATC CTC AAT CTT CAG GAA CTC CGC GTC AAT G-3') that anneals at the IDCL region of NcPCNA ORF. The PCR product was digested with SphI restriction enzyme and was used to replace a similar fragment in the pUC19-NcPCNA construct. Similarly, two NcPCNA mutants (NcPCNA-J and NcPCNA-IDCL2-J) with J loop substitutions were made. Residues S105, S106, E107, and N108 of NcPCNA were mutated to D, T, K, and K residues, respectively, to mimic the J loop of ScPCNA by using a mutagenic forward primer NAP812 (5'-CCT CGT CTT CGA AGA TAC CAA AAA GGA CCG TAT C-3') and M13 reverse primer that anneals to a sequence downstream to the EcoRI site of pUC19. The PCR product was digested with BstBI-EcoRI and was used to replace a similar fragment in NcPCNA. Respective mutants were sequenced, and further, they were cloned under *S. cerevisiae ADH1* promoter for genetic analyses.

Purification of recombinant proteins

The expression of ScPCNA, ScPCNA G178S, and NcPCNA proteins was carried out in *Escherichia coli* BL21 DE3 cells. The proteins were expressed either as GST- or His-tag fusion proteins under the T7 promoter using a protocol described previously (9, 26, 27). PCNA was cleaved off from GST-bound beads after overnight incubation with PreScission Protease (GE Healthcare). His-NcPCNA was purified for crystallization purpose using HisTrap FF 5-ml nickel affinity column connected to an AKTA Pure 25 M protein purification system (GE Healthcare) and equilibrated with a buffer containing 50 mM Tris HCl (pH 7.5), 500 mM sodium chloride, 0.05% NP-40, 1 mM β-mercaptoethanol, 1 mM PMSF, and one EDTA-free protease inhibitor cocktail tablet (Roche). The NcPCNA

bound to the column was eluted out using a 0 to 500 mM imidazole linear gradient. The peak fractions were checked on an 18% SDS-PAGE gel. Pure fractions were pooled together and concentrated to about 5 ml using a 10-kDa cut-off Amicon Ultra-15 Centrifugal Filter and loaded onto a HiLoad 16/600 Superdex 200 pg size-exclusion column equilibrated with a buffer containing 20 mM Tris HCl (pH 7.5), 100 mM NaCl, and 1 mM DTT. The homogeneity of the purified recombinant protein obtained from the peak fractions was analyzed on an 18% SDS-PAGE gel. The fractions containing pure recombinant His-NcPCNA were pooled together, concentrated with the help of a 10-kDa cut-off Amicon Ultra-15 Centrifugal Filter to 15 mg/ml, aliquoted, and stored at -80°C , after flash-freezing in liquid nitrogen. Purified proteins were estimated by both Bradford's and gel-based assay using bovine serum albumin as a standard. The proteins were also analyzed by electrophoresis on 12% polyacrylamide gels with or without 2 M urea (28) and visualized by Coomassie Brilliant Blue R-250 staining.

ScPol32 was also purified using the protocol mentioned above, except that a GAL-PGK-GST-ScPol32 construct was expressed in YRP654 yeast strain (29).

Analytical size-exclusion chromatography

For analytical size-exclusion chromatography, about 10 μg of purified proteins was loaded onto a Superdex 200 PC3.2/30 column pre-equilibrated with the buffer containing 50 mM Hepes (pH 7.5), 150 mM NaCl, and 10% glycerol with or without 2 M urea. Chromatography was performed on an AKTA Pure 25 M system at a flow rate of 0.05 ml/min at 4°C , and the absorbance was monitored at 280 nm.

Crystallization and data collection

Crystallization screening of NcPCNA at a concentration of 15 mg/ml was performed using commercially available sparse matrix screens from Hampton Research and Jena Bioscience with the help of an NT8 crystallization robot (Formulatrix) in 96-well MRC plates, similar to that of CaPCNA (9). The plates were incubated at 18°C in a crystallization incubator. Ten days later, hexagonal crystals were observed in a condition containing 0.2 M calcium acetate (pH 7.5) and 20% PEG3350. Diffraction quality crystals were obtained by mixing 1.5 μl of protein (8 mg/ml) and 1 μl of the crystallization condition in a 24-well hanging drop vapor diffusion plate at 18°C . The crystals were cryoprotected with 20% ethylene glycol and flash-frozen in liquid nitrogen. High-resolution datasets were recorded on the MAR mosaic 225 mm CCD detector of the PX-BL21 beamline at Indus-2, RRCAT, Indore, India (30), at 0.9537 \AA X-ray wavelength. The diffraction images were indexed and integrated with the iMOSFLM program. The crystal belonged to the *H3* space group with $a = 86.29 \text{ \AA}$, $b = 86.29$, $c = 91.94 \text{ \AA}$, and α and $\beta = 90^{\circ}$, $\gamma = 120^{\circ}$ as unit cell dimensions. Consequently, the datasets were scaled and merged using the program AIMLESS (31). A Matthews coefficient value of $2.26 \text{ \AA}^3/\text{Da}$ indicated one monomer of

NcPCNA in an ASU, with 45% solvent content. The data quality estimation using Xtriage from Phenix (32) revealed merohedral twinning with a twin fraction of 0.192.

Crystal structure solution and refinement

NcPCNA structure was solved by molecular replacement, using the AfPCNA structure as a search model (PDB ID: 5TUP) with Phaser-MR in Phenix suite (32), which found one protomer of NcPCNA in the ASU. Because the crystal was twinned, twin refinement was performed using Phenix.refine (32) by applying the twinning operator $h, -h, -k, -l$. Subsequently, manual model building was carried out in Coot (33), and the final refined structure gave R and R_{free} values of 19.6 and 23.5, respectively. The stereochemical quality of the final refined structure was analyzed using the program MolProbity (34). The data collection summary and refinement statistics are provided in Table 1. The molecular graphics and coloring were ray-traced using UCSF Chimera and PyMOL (Schrödinger, LLC). The surface electrostatic charge potentials were calculated using the Adaptive Poisson-Boltzmann Solver software (35).

Complementation analysis by plasmid curing

YTS9, a genomic *POL30* null strain of *S. cerevisiae* that survives by episomal expression of a mutant ScPCNA (CEN-ScPOL30 D41 A, D42A-*TRP1*), was used for the heterologous PCNA complementation assay. Plasmids YCplac33-ScADH1p (CEN, *URA3*) expressing ScPCNA or NcPCNA ORFs were transformed into YTS9 strain, and the transformants were selected on synthetic media without tryptophan and uracil (15). In these constructs, PCNA is expressed under *S. cerevisiae* *ADH1* constitutive promoter. For the control experiment, an empty vector was also transformed. To cure the resident plasmid containing mutant ScPOL30 (YCP-ScPOL30 D41A, D42A, *TRP1*) from YTS9 transformants, a transformant from each plate was grown on liquid media omitting uracil at 30°C in the shaking condition. After every 24 h, 100 μl of the culture was added to fresh 6 ml of SD medium without uracil and allowed to grow. After five consecutive subcultures, the cultures were streaked on SD plates without uracil to obtain isolated colonies. About 20 isolated colonies were patched on SD agar plates lacking uracil alone or tryptophan alone to check the curing efficiency. Furthermore, the plates were incubated at 30°C for 2 days and the number of colonies that appeared on each plate was counted. The lack of growth on the SD-tryptophan plate but growth on SD-uracil suggests complete curing of the resident PCNA and complementation by PCNA present on the incoming plasmid. On the other hand, preservation of both the nutritional markers (uracil and tryptophan) indicates that the tester plasmid cannot complement ScPOL30. After curing, the strains were confirmed by PCR for the presence of respective plasmids.

Plasmid segregation by 5-FOA counterselection

Yeast strain YNA11 is a genomic null for *POL30* but harbors YEplac195-ScADH1p-ScPol30 (2 μ , *URA3*). An empty

Three-dimensional structure of NcPCNA

YEplac181-ScADH1p (2 μ , *LEU2*) vector or that containing ScPCNA or NcPCNA or the mutants of NcPCNA were transformed into the above strain. The transformants were selected on SD media without leucine and uracil. Isolated colonies were picked and restreaked on an SD-leucine agar plate but with or without 5-FOA (1 mg/ml). After counter-selection with 5-FOA, the absence of original PCNA in strains surviving on FOA-containing plate was confirmed by PCR. Simultaneously, plasmid bumping of various transformants was also carried out, as mentioned above, by continuous subculturing in liquid media, omitting leucine to verify complementation.

Growth rates

Growth rates for yeast strains were examined by inoculating 1 ml of preculture to 100 ml fresh YPD liquid medium. About 1 ml culture was taken out every 2 h for 18 h, and the growth rate at 30 °C was monitored by measuring absorbance at 600 nm. The experiment was repeated twice with three replicates.

Sensitivity to genotoxic agents

All the precultures of the various strains were diluted to achieve an equal number of cells in autoclaved water. Furthermore, these strains were 10-fold serially diluted and spotted on YPD plates with or without different concentrations of drugs such as HU (0–50 mM), MMS (0–0.0018%), and H₂O₂ (0–4 mM). The plates were incubated at 30 °C for 2 days and then photographed. For UV treatment, the spotted YPD plates were exposed to different doses of UV radiation (0–18 J/m²), covered with aluminum foil, and then incubated.

For quantitative survival experiments, logarithmically growing cells were diluted to about 500 cells/ml, from which 200 μ l was spread onto YPD plates with or without DNA-damaging agents at indicated concentrations. For UV treatment, the plates were exposed to UV irradiation of different doses. After 2- to 3-days of incubation, the number of colonies on each plate was counted.

ITC

NcPCNA, ScPCNA, and ScPol32 were dialyzed against a buffer containing 20 mM Hepes (pH 7.5), 150 mM NaCl, and 1 mM β -mercaptoethanol. Protein concentrations were measured at an absorbance of 280 nm using the respective extinction coefficients and molecular mass. T2AA (Sigma-Aldrich) was dissolved in 100% DMSO to a concentration of 9.14 mM and further diluted to 600 μ M with the dialysis buffer. NcPCNA and ScPCNA were diluted to 30 μ M in the dialysis buffer, and 6.6% DMSO was added to both the protein solutions to avoid buffer mismatch. ITC experiments were performed using a MicroCal PEAQ-ITC system (Malvern Panalytical) with 30 μ M ScPol32 loaded into the sample cell and 150 μ M ScPCNA or 300 μ M NcPCNA injected from the syringe. For T2AA binding, 30 μ M NcPCNA/ScPCNA was loaded into the sample cell, and 600 μ M T2AA was injected from the syringe. 25 consecutive injections (1.5 μ l each) were

made at an interval of 120 s and mixed at 750 rpm at 25 °C. Control experiments were performed, wherein the heat of dilution of T2AA or ScPol32 into a buffer and the buffer into the buffer were subtracted from the respective individual experiments. Binding isotherms were fitted into a one-site binding model using the MicroCal PEAQ-ITC Analysis software (Malvern Panalytical). All the experiments were performed in triplicates, and the calculated binding affinity, change in enthalpy, and entropy were consistent.

Data availability

Coordinate and structure factor files for NcPCNA have been deposited in the Protein Data Bank with the accession code 7EP8.

Supporting information—This article contains [supporting information](#).

Acknowledgments—We thank our laboratory members for critically reading the manuscript. We are also grateful to Ms Mousumi Sajjan for initiating the project.

Author contributions—P. K., R. S., K. M., D. V., and N. A. resources; P. K., R. S., K. M., and N. A. data curation; P. K., R. S., D. V., and N. A. formal analysis; P. K., R. S., K. M., D. V., and N. A. validation; P. K., R. S., K. M., D. V., and N. A. methodology; P. K., R. S., K. M., D. V., and N. A. writing—original draft; P. K., R. S., K. M., D. V., and N. A. writing—review and editing; R. S., K. M., D. V., and N. A. software; K. M., D. V., and N. A. investigation; K. M., D. V., and N. A. visualization; D. V. and N. A. supervision; D. V. and N. A. funding acquisition; N. A. conceptualization; N. A. project administration.

Funding and additional information—The research fellowship from the Department of Biotechnology, Government of India, to R. S. and the intramural and extramural supports from the Institute of Life Sciences, DBT, and SERB at different times of the study to D. V. and N. A. are greatly acknowledged.

Conflict of interest—The authors declare that they have no conflicts of interest with the contents of this article.

Abbreviations—The abbreviations used are: 5-FOA, 5-fluoroorotic acid; AfPCNA, *A. fumigatus* PCNA; ASU, asymmetric unit; CaPCNA, *C. albicans* PCNA; FOA, fluoroorotic acid; HU, hydroxyurea; HsPCNA, human PCNA; IDCL, interdomain connecting loop; ITC, isothermal titration calorimetry; MMS, methyl methanesulfonate; NcPCNA, *N. crassa* PCNA; PCNA, proliferating cell nuclear antigen; PIP, PCNA-interacting peptide; ScPCNA, *S. cerevisiae* PCNA; SD, synthetic defined; SpPCNA, *S. pombe* PCNA; T2AA, T2-amino alcohol; YPD, yeast extract, peptone, dextrose.

References

1. Acharya, N., Patel, S. K., Sahu, S. R., and Kumari, P. (2020) 'PIPs' in DNA polymerase: PCNA interaction affairs. *Biochem. Soc. Trans.* **48**, 2811–2822
2. Maga, G., and Hubscher, U. (2003) Proliferating cell nuclear antigen (PCNA): A dancer with many partners. *J. Cell Sci.* **116**, 3051–3060

3. Acharya, N., Klassen, R., Johnson, R. E., Prakash, L., and Prakash, S. (2011) PCNA binding domains in all three subunits of yeast DNA polymerase delta modulate its function in DNA replication. *Proc. Natl. Acad. Sci. U. S. A.* **108**, 17927–17932
4. Khandagale, P., Thakur, S., and Acharya, N. (2020) Identification of PCNA-interacting protein motifs in human DNA polymerase delta. *Biosci. Rep.* **40**, BSR20200602
5. Khandagale, P., Peroumal, D., Manohar, K., and Acharya, N. (2019) Human DNA polymerase delta is a pentameric holoenzyme with a dimeric p12 subunit. *Life Sci. Alliance* **2**, e201900323
6. Manohar, K., and Acharya, N. (2015) Characterization of proliferating cell nuclear antigen (PCNA) from pathogenic yeast *Candida albicans* and its functional analyses in *S. cerevisiae*. *BMC Microbiol.* **15**, 257
7. Krishna, T. S., Fenyo, D., Kong, X. P., Gary, S., Chait, B. T., Burgers, P., and Kuriyan, J. (1994) Crystallization of proliferating cell nuclear antigen (PCNA) from *Saccharomyces cerevisiae*. *J. Mol. Biol.* **241**, 265–268
8. Krishna, T. S., Kong, X. P., Gary, S., Burgers, P. M., and Kuriyan, J. (1994) Crystal structure of the eukaryotic DNA polymerase processivity factor PCNA. *Cell* **79**, 1233–1243
9. Sundaram, R., Manohar, K., Patel, S. K., Acharya, N., and Vasudevan, D. (2021) Structural analyses of PCNA from the fungal pathogen *Candida albicans* identify three regions with species-specific conformations. *FEBS Lett.* **595**, 1328–1349
10. Marshall, A. C., Kroker, A. J., Murray, L. A., Gronthos, K., Rajapaksha, H., Wegener, K. L., and Bruning, J. B. (2017) Structure of the sliding clamp from the fungal pathogen *Aspergillus fumigatus* (AfumPCNA) and interactions with human p21. *FEBS J.* **284**, 985–1002
11. Zamir, L., Zaretsky, M., Fridman, Y., Ner-Gaon, H., Rubin, E., and Aharoni, A. (2012) Tight coevolution of proliferating cell nuclear antigen (PCNA)-partner interaction networks in fungi leads to interspecies network incompatibility. *Proc. Natl. Acad. Sci. U. S. A.* **109**, E406–E414
12. Freudenthal, B. D., Ramaswamy, S., Hingorani, M. M., and Washington, M. T. (2008) Structure of a mutant form of proliferating cell nuclear antigen that blocks translesion DNA synthesis. *Biochemistry* **47**, 13354–13361
13. Dieckman, L. M., and Washington, M. T. (2013) PCNA trimer instability inhibits translesion synthesis by DNA polymerase eta and by DNA polymerase delta. *DNA Repair* **12**, 367–376
14. Gonzalez-Magana, A., and Blanco, F. J. (2020) Human PCNA structure, function and interactions. *Biomolecules* **10**, 570
15. Ayyagari, R., Impellizzeri, K. J., Yoder, B. L., Gary, S. L., and Burgers, P. M. (1995) A mutational analysis of the yeast proliferating cell nuclear antigen indicates distinct roles in DNA replication and DNA repair. *Mol. Cell. Biol.* **15**, 4420–4429
16. Arroyo, M. P., Downey, K. M., So, A. G., and Wang, T. S. (1996) *Schizosaccharomyces pombe* proliferating cell nuclear antigen mutations affect DNA polymerase delta processivity. *J. Biol. Chem.* **271**, 15971–15980
17. Ng, L., Prelich, G., Anderson, C. W., Stillman, B., and Fisher, P. A. (1990) *Drosophila* proliferating cell nuclear antigen. Structural and functional homology with its mammalian counterpart. *J. Biol. Chem.* **265**, 11948–11954
18. Gibbs, E., Kelman, Z., Gulbis, J. M., O'Donnell, M., Kuriyan, J., Burgers, P. M., and Hurwitz, J. (1997) The influence of the proliferating cell nuclear antigen-interacting domain of p21(CIP1) on DNA synthesis catalyzed by the human and *Saccharomyces cerevisiae* polymerase delta holoenzymes. *J. Biol. Chem.* **272**, 2373–2381
19. Acharya, N., Manohar, K., Peroumal, D., Khandagale, P., Patel, S. K., Sahu, S. R., and Kumari, P. (2019) Multifaceted activities of DNA polymerase eta: Beyond translesion DNA synthesis. *Curr. Genet.* **65**, 649–656
20. Acharya, N., Khandagale, P., Thakur, S., Sahu, J. K., and Utkalaja, B. G. (2020) Quaternary structural diversity in eukaryotic DNA polymerases: Monomeric to multimeric form. *Curr. Genet.* **66**, 635–655
21. Manohar, K., Peroumal, D., and Acharya, N. (2018) TLS dependent and independent functions of DNA polymerase eta (Poleta/Rad30) from pathogenic yeast *Candida albicans*. *Mol. Microbiol.* **110**, 707–727
22. Acharya, N., Haracska, L., Johnson, R. E., Unk, I., Prakash, S., and Prakash, L. (2005) Complex formation of yeast Rev1 and Rev7 proteins: A novel role for the polymerase-associated domain. *Mol. Cell. Biol.* **25**, 9734–9740
23. Gohain, D., and Tamuli, R. (2019) Calcineurin responsive zinc-finger-1 binds to a unique promoter sequence to upregulate neuronal calcium sensor-1, whose interaction with MID-1 increases tolerance to calcium stress in *Neurospora crassa*. *Mol. Microbiol.* **111**, 1510–1528
24. Notredame, C., Higgins, D. G., and Heringa, J. (2000) T-coffee: A novel method for fast and accurate multiple sequence alignment. *J. Mol. Biol.* **302**, 205–217
25. Robert, X., and Gouet, P. (2014) Deciphering key features in protein structures with the new ENDscript server. *Nucleic Acids Res.* **42**, W320–W324
26. Johnson, R. E., Prakash, L., and Prakash, S. (2006) Yeast and human translesion DNA synthesis polymerases: Expression, purification, and biochemical characterization. *Methods Enzymol.* **408**, 390–407
27. Acharya, N., Brahma, A., Haracska, L., Prakash, L., and Prakash, S. (2007) Mutations in the ubiquitin binding UBZ motif of DNA polymerase eta do not impair its function in translesion synthesis during replication. *Mol. Cell. Biol.* **27**, 7266–7272
28. Acharya, N., Roy, S., and Varshney, U. (2002) Mutational analysis of the uracil DNA glycosylase inhibitor protein and its interaction with *Escherichia coli* uracil DNA glycosylase. *J. Mol. Biol.* **321**, 579–590
29. Acharya, N., Johnson, R. E., Pages, V., Prakash, L., and Prakash, S. (2009) Yeast Rev1 protein promotes complex formation of DNA polymerase zeta with Pol32 subunit of DNA polymerase delta. *Proc. Natl. Acad. Sci. U. S. A.* **106**, 9631–9636
30. Kumar, A., Ghosh, B., Poswal, H. K., Pandey, K. K., Jagannath, Hosur, M. V., Dwivedi, A., Makde, R. D., and Sharma, S. M. (2016) Protein crystallography beamline (PX-BL21) at Indus-2 synchrotron. *J. Synchrotron Radiat.* **23**, 629–634
31. Evans, P. R., and Murshudov, G. N. (2013) How good are my data and what is the resolution? *Acta Crystallogr. D Biol. Crystallogr.* **69**, 1204–1214
32. Adams, P. D., Afonine, P. V., Bunkoczi, G., Chen, V. B., Davis, I. W., Echols, N., Headd, J. J., Hung, L. W., Kapral, G. J., Grosse-Kunstleve, R. W., McCoy, A. J., Moriarty, N. W., Oeffner, R., Read, R. J., Richardson, D. C., et al. (2010) PHENIX: A comprehensive Python-based system for macromolecular structure solution. *Acta Crystallogr. D Biol. Crystallogr.* **66**, 213–221
33. Emsley, P., and Cowtan, K. (2004) Coot: Model-building tools for molecular graphics. *Acta Crystallogr. D Biol. Crystallogr.* **60**, 2126–2132
34. Chen, V. B., Arendall, W. B., 3rd, Headd, J. J., Keedy, D. A., Immormino, R. M., Kapral, G. J., Murray, L. W., Richardson, J. S., and Richardson, D. C. (2010) MolProbity: All-atom structure validation for macromolecular crystallography. *Acta Crystallogr. D Biol. Crystallogr.* **66**, 12–21
35. Unni, S., Huang, Y., Hanson, R. M., Tobias, M., Krishnan, S., Li, W. W., Nielsen, J. E., and Baker, N. A. (2011) Web servers and services for electrostatics calculations with APBS and PDB2PQR. *J. Comput. Chem.* **32**, 1488–1491